Aus dem Zentrum für Innere Medizin der Universität zu Köln
Klinik und Poliklinik für Innere Medizin II der Universität zu Köln
Direktor: Universitätsprofessor Dr. med. Th. Benzing

The role of GLIS2 in maintenance of genome integrity in the development of nephronophthisis

Inaugural-Dissertation zur Erlangung der Doktorwürde
der Medizinischen Fakultät
der Universität zu Köln

vorgelegt von
Lukas Schlößer
aus Bergisch Gladbach

promoviert am 21. November 2022

Gedruckt mit Genehmigung der Medizinischen Fakultät der Universität zu Köln
2022

Dekan: Universitätsprofessor Dr. med. G. R. Fink
1. Gutachter: Professor Dr. med. B. Schermer
2. Gutachter: Universitätsprofessor Dr. rer. nat. B. Schumacher

Erklärung

Ich erkläre hiermit, dass ich die vorliegende Arbeit ohne unzulässige Hilfe Dritter und ohne Benutzung anderer als der angegebenen Hilfsmittel angefertigt habe; die aus fremden Quellen direkt oder indirekt übernommenen Gedanken sind als solche kenntlich gemacht.

Bei der Auswahl und Auswertung des Materials sowie bei der Herstellung des Manuskriptes habe ich Unterstützungsleistungen von folgenden Personen erhalten:

Gisela Slaats, Ph.D.
Prof. Dr. med. Bernhard Schermer

Weitere Personen waren an der geistigen Herstellung der vorliegenden Arbeit nicht beteiligt. Insbesondere habe ich nicht die Hilfe einer Promotionsberaterin/ eines Promotionsberaters in Anspruch genommen. Dritte haben von mir weder unmittelbar noch mittelbar geldwerte Leistungen für Arbeiten erhalten, die im Zusammenhang mit dem Inhalt der vorgelegten Dissertationsschrift stehen.

Die Dissertationsschrift wurde von mir bisher weder im Inland noch im Ausland in gleicher oder ähnlicher Form einer anderen Prüfungsbehörde vorgelegt.

Die in dieser Arbeit angegebenen Experimente sind nach entsprechender Anleitung durch Frau Gisela Slaats, PhD (Betreuerin) und Herrn Prof. Dr. med. Bernhard Schermer (Doktorvater) von mir selbst ausgeführt worden.

Die Immunisierung von Mäusen zur Generierung von peptidspezifischen Antikörpern im Rahmen dieser Arbeit wurde von Frau Gisela Slaats, Ph.D. vorgenommen. Die Generierung sowie Kultivierung von Hybridoma-Zellen im Rahmen dieser Arbeit wurde von Herrn Prof. Dr. Bernhard Schermer durchgeführt.

Die massenspektrometrische Analyse von Immunpräzipitaten wurde ohne meine Mitarbeit im Labor der Proteomics facility des CECAD Köln durchgeführt. Die nachfolgende bioinformatische Prozessierung der bioinformatischen Rohdaten wurde von Herrn Dr. rer. nat. Christian Freese vorgenommen.

Erklärung zur guten wissenschaftlichen Praxis:

Ich erkläre hiermit, dass ich die Ordnung zur Sicherung guter wissenschaftlicher Praxis und zum Umgang mit wissenschaftlichem Fehlverhalten (Amtliche Mitteilung der Universität zu Köln AM 132/2020) der Universität zu Köln gelesen habe und verpflichte mich hiermit, die dort genannten Vorgaben bei allen wissenschaftlichen Tätigkeiten zu beachten und umzusetzen.

Köln, den 17.02.2022

Unterschrift:

Danksagung

An dieser Stelle möchte ich den Personen danken, welche diese Arbeit durch ihre Unterstützung erst möglich gemacht haben.

Zunächst möchte ich mich bei Herrn Universitätsprofessor Dr. Thomas Benzing bedanken, dass ich die Möglichkeit erhielt im nephrologischen Forschungslabor seiner Klinik in einem sehr strukturierten und bestens ausgestatteten Arbeitsumfeld mit einem äußerst kompetenten und freundlichen Team an der im Rahmen dieser Arbeit behandelten Fragestellung forschen zu dürfen.

Ein besonderer Dank gilt meinem Doktorvater Herrn Professor Dr. Bernhard Schermer, welcher durch stetige kritische und konstruktive Revision die Entstehung dieser Arbeit gefördert und durch seine Begeisterung und wissenschaftliche Neugier meine Motivation stets befeuert hat.

Nicht zuletzt möchte ich ganz besonders meiner Betreuerin Frau Gisela Slaats, Ph.D. danken deren Betreuung meiner Person durch eine außerorderntliche Klarheit und Geduld geprägt war und welche mich in die experimentelle Arbeit im Labor und an hohe wissentschaftliche Standards herangeführt hat. Darüber hinaus unterstützte sie mich stets durch wertvolle Anregungen und positive Impulse bei der Bearbeitung der dieser Arbeit zugrundeliegenden Fragestellung.

Des Weiteren bedanke ich mich bei dem gesamten Team des Nephrolabors für eine spannende, lehrreiche und vor allem schöne Zeit.

Schließlich spreche ich meine tief empfundene Dankbarkeit meiner Familie für die bedingungslose Unterstützung und die Nachsicht, welche mir in herausfordernden Phasen meines Studiums und dieser Arbeit entgegengebracht wurde, aus.

Meinen Eltern.

Content

Abbreviations

%	per cent
3'/5'	3 prime/ 5 prime
°C	degrees Celsius
µ	micro
aa	Amino acids
AAV	Adeno-associated virus
ACTN1/4	Alpha-actinin 1/4
ADP	adenosine-diphosphate
ADPKD	autosomal dominant polycystic kidney disease
AMPK	AMP-dependent kinase
APC	adenomatous polyposis coli
APEX	ascorbate peroxidase
APS	ammonium persulfate
ARPKD	autosomal recessive polycystic kidney disease
Asp	asparagine
ATM	Ataxia telangiectasia mutated
ATP	adenosine triphosphate
ATR	Ataxia telangiectasia and Rad3 related
ATRIP	ATR interacting protein
BBS	Bardet Biedl syndrome
Bp	base pairs
BSA	bovine serum albumin
Ca	calcium
CAA	Chloroacetamide
cAMP	cyclic AMP
cDNA	coding DNA
CDC42	Cell division control protein 42 homolog
CED	Cranioectodermal Dysplasia
CEP164	centrosomal protein 164 kDa
CEP290	centrosomal protein 290 kDa
CFTR	cystic fibrosis transmembrane conductance regulator
ChIP-seq	Chromatin Immunoprecipitation DNA-Sequencing
CHK1/2	checkpoint kinase 1/2
CK1	casein kinase 1
Cl	Chloride

CLS	ciliary localization signal
CNS	central nervous system
CO_2	Carbon trioxide
CRISPR	Clustered Regularly Interspaced Short Palindromic Repeats
CTNND1	Catenin delta-1
Ctrl	control
CTTN	Src substrate cortactin
DAPI	4′, 6-diamidino-2-phenylindole
ddH_2O	Double-distilled water
DDR	DNA damage response
DMEM	Dulbecco's Modified Eagle's Medium
DNA	Deoxyribonucleic acid
DNA-PKcs	DNA-dependent protein kinase (catalytic subunit)
DSB	double strand break
DTT	Dithiothreitol
EDTA	Ethylenediaminetetraacetic acid
e.g.	exempli gratia
ELISA	Enzyme-linked Immunosorbent Assay
EMT	epithelial-mesenchymal-transition
ESRD	end stage renal disease
et al.	and others
F	fluorine
FACS	fluorescence activated cell sorting
Fc	fragment crystallized
FDR	false discovery rate
Fig.	figure
FL	full length
Fp	forward primer
G	gramm
g	gravity
GBS	Gli-binding site
GFP	Green fluorescent protein
GFR	Glomerular filtration rate
GLI1/2/3	Zinc finger protein GLI1/2/3
GliA	activated GLI
GlisBS	GLIS2 binding sequence
GLIS2	Gli-similar family zinc finger 2

GO	gene ontology
GSK-3β	glycogen synthase kinase 3β
GSN	Gelsolin
GST	glutathione-S-transferase
GTP	guanosine triphosphate
h	hour
h	human
H	Hydrogen
HAT	hypoxanthine-aminopterin-thymidine
HeBS	HEPES-buffered saline
HEK	human embryonic kidney
HeLa	Henrietta Lacks
HEPES	4-(2-hydroxyethyl)-1-piperazineethanesulfonic acid
HGPRT	hypoxanthine guanine phosphoribosyl transferase
Hh	Hedgehog
HSP90AA1/B1	Heat Shock Protein 90 Alpha Family Class A/B Member 1
IF	Immunofluorescence
IFT	Intraflagellar transport
Ig	Immunoglobuline
IL-6	Interleukine 6
IMCD	Inner medullary collecting duct
iNOS	inducible nitric oxide synthases
IP	Immunoprecipitation
IPTG	Isopropyl β-D-1-thiogalactopyranoside
JATD	Jeune Asphyxiating Thoracic Dystrophy
JBTS	Joubert Syndrome
K	Potassium
Kb	kilobases
kDa	kilodalton
KI	knock-in
KIF7	Kinesin family member 7
Ksp	kidney specific
l	Liter
LB	Lysogeny broth
LFQ	Label-free quantification
LIG3/4	DNA ligase 3/4
LKB1	Liver kinase B1

log	Logarithmus
m	Meter
m	mouse
M	Molar
M2	Anti-FLAG monoclonal
mA	miliampere
MAPKBP1	MAP kinase-binding protein 1
MDCK	Madin-Darby Canine Kidney
MHC1	Major histocompatibility complex 1
MKS	Meckel Grüber Syndrome
min	minutes
ml	millilitre
MRE11	Meiotic recombination 11
MRN	MRE11, RAD50 and NBS1
mRNA	messenger RNA
MS	Mass spectrometry
mTOR	Mammalian target of rapamycin
MYO9/10/14	Myosin 9/10/14
n	nano
Na	Sodium
NBS1	Nijmegen breakage syndrome 1
NDS	Normal donkey serum
NEK8	NIMA Related Kinase 8
NEMO	NF-κB essential modulator
NF-κB	nuclear factor 'kappa-light-chain-enhancer' of activated B-cells
nLC	Nano-liquid-chromatography
NP-40	Nonyl phenoxypolyethoxylethanol
NPH	Nephronophthisis
NPHP	Nephronophthisis protein
NPHP-RC	Nephronophthisis protein-related ciliopathy
OCT	Optimal cutting temperature
OFD	Oro facial dysmorphism
PAR	Poly-ADP-ribose
PARP1	Poly (ADP-ribose) polymerase 1
PBS	Phosphate-buffered saline
PBST	Phosphate-buffered saline + Tween 20
PC-1/-2	Polycystin 1/2

PCR	poly chain reaction
PEG	Polyethylene glycol
PFA	Paraformaldehyde
pH	$-\log_{10}(H^{+})$
PIASy	E3 SUMO-protein ligase PIAS4
PIM	protease inhibitor mix
PKD1/2	Polycystic kidney disease 1
PKHD1	Fibrocystin
PMSF	phenylmethylsulfonyl fluoride
PO_4	phosphate
PTCH	Patched
PVDF	Polyvinylidene difluoride
qPCR	quantitive PCR
RAD50	DNA repair protein RAD50
RHEB	Ras homolog enriched in brain
RIPA	Radioimmunoprecipitation assay buffer
RISC	RNA-induced silencing complex
RNA	Ribonucleic acid
Rp	reverse primer
Rpm	rounds per minute
RPA	Replication protein A
s	Second
SDCCAG8	Serologically Defined Colon Cancer Antigen 8
SDS	Sodium dodecyl sulfate
sgRNA	guide RNA
siRNA	short interfering RNA
SLS	Senior Loken syndrome
SMO	Smoothened
SOC	Super Optimal broth with Catabolite repression
S-phase	Synthesis-phase
SRP	Short Rib Polydactyly
SSB	single strand break
ssODN	single stranded oligodeoxynucleotide
SUFU	Suppressor of fused
TALEN	Transcription activator-like effector nuclease
TAZ	Transcriptional coactivator with PDZ-binding motif
TEMED	N,N,N',N'-tetramethylethane-1,2-diamine

TGF-β	Transforming growth factor beta
TMB	3,3',5,5'-Tetramethylbenzidine
TNF-α	Tumor necrosis factor alpha
TNPO1	Transportin 1
TPM1/3/4	Tropomyosin 1/3/4
TSC-1/2	Tuberous sclerosis 1/2
U2OS	human osteosarcoma cell line
UV	Ultraviolette
V	Volt
WB	Western blot
Wnt	Wingless-Int
WT	Wild-type
XRCC5/6	X-ray cross complementing protein 5/6
YAP	Yes-associated protein 1
γH2AX	phosphorylated (S139) histone 2A, family member X
ZNF423	zinc finger protein 423

1. Summary

Nephronophthisis (NPH) is an autosomal-recessive inherited ciliopathy and the most common genetically determined cause of end-stage renal disease in early childhood [99]. Kidney failure is due to the development of excessive fibrosis and cysts at the corticomedullary border in the kidneys of these patients, which replace the functional kidney tissue [99]. Today mutations in ≥20 different genes have been identified to cause NPH [99]. The pathogenesis of NPH seems to be complex and to differ among the NPH subtypes, as well as the exact mechanisms remain largely unknown so far [134].

One unifying concept is the presence of almost all NPH proteins at the base of or in primary cilia [99]. In 2012 the first link between two NPH proteins (ZNF423 and CEP164) and the DDR pathway was identified, providing a new perspective on the pathogenesis of NPH [19]. This finding led to the hypothesis that the DDR in cells lacking one of those NPH proteins is impaired, making the cell more susceptible to genotoxic influences like extracellular genotoxic substances or replication stress leading to the accumulation of DNA damage [19]. This accumulation of DNA damage leads to the induction of cellular programs such as apoptosis and cellular senescence [16]. Furthermore, DNA damage is also a trigger for the innate immune response, which might cause immune cell infiltration in the kidney tissue, providing a profibrotic environment for the tubule epithelial cells in the context of NPH, thus promoting EMT [105,113]. Seven NPH proteins have been linked to roles in the DDR so far [3,19,24,98,102,133].

We focused on GLIS2, which has been identified as NPHP7 [7]. Because of its primary localization in the nucleus, its known functions in the regulation of transcription, and the finding of activated DDR in GLIS2 knock-out cells, it was reasonable to assume that GLIS2 also plays a crucial role in the DDR [98,145]. We generated the first GLIS2 interactome derived from mass spectrometry-based analysis of immunoprecipitates from stable cell lines expressing low levels of wild-type GLIS2 and two truncations. Interestingly, this revealed key components of DDR pathways like PARP1, DNA-PKcs, and RAD50 [16,105]. These data support a potential role of GLIS2 in the DDR and thus in the maintenance of genome integrity. Furthermore, many ciliary proteins were also found in this interactome, providing evidence for a ciliary localization of GLIS2.

1.1. Zusammenfassung

Nephronophthise (NPH) ist eine autosomal-rezessiv vererbte Erkrankung aus der Gruppe der Ziliopathien und die häufigste genetisch-bedingte Ursache einer Niereninsuffizienz im Kindesalter [99]. Die Entstehung der Niereninsuffizienz bei diesen Patienten ist durch eine massive Fibrose des Nierengewebes und die Ausbildung von Zysten am kortikomedullären Übergang bedingt [99]. Bis jetzt wurden Mutationen in ≥20 verschiedenen Genen als ursächlich identifiziert [99]. Die Pathogenese der NPH ist komplex, scheint zwischen den unterschiedlichen Subtypen zu divergieren und ist weitestgehend unverstanden [134]. Eine Gemeinsamkeit ist das Vorhandensein von fast allen NPH-Proteinen an der Basis des Primärziliums oder im ziliären Kompartiment [99]. Im Jahre 2012 erschien die erste Publikation, welche zwei NPH-Proteine (ZNF423 und CEP164) mit Funktionen im Rahmen des DDR in Verbindung brachte und dadurch eine neue Perspektive auf die Pathogenese der NPH eröffnete [19]. Auf Basis dessen wurde die Hypothese formuliert, dass Zellen, in denen eines der NPH-Proteine fehlt und damit der DDR beeinträchtigt ist, anfälliger für gentoxische Einflüsse sind, was schließlich zur Akkumulation von DNA-Läsionen führt [19]. Die Akkumulation von DNA-Läsionen führt zur Initiation zellulärer Programme wie Apoptose oder zellulärer Seneszenz [16]. Darüber hinaus stellen DNA-Läsionen einen Stimulus für die Aktivierung des angeborenen Immunsystems dar, was zu einer Immunzellinfiltration des Nierengewebes führen könnte und dadurch eine profibrotische Umgebung für tubuläre Epithelzellen und deren epithelial-mesenchymale Transition bedingen könnte [16,105,113]. Bisher sind sieben NPH-Proteine mit Funktionen im Rahmen des DDR in Verbindung gebracht worden [3,19,24,98,102,133]. Im Mittelpunkt dieser Arbeit steht GLIS2, welches - im Falle einer Mutation - zu NPH Typ 7 führt [7]. Aufgrund seiner nukleären Lokalisation und dessen bereits bekannten Funktionen im Rahmen der Regulierung der Transkription von verschiedenen Genen und eines aktivierten DDR in GLIS2 knock-out Zellen, liegt es nahe zu vermuten, dass GLIS2 wichtige Funktionen im DDR besitzt [145]. Dazu wurde das erste GLIS2-Interactom, basierend auf der massenspektrometrischen Analyse von Immunpräzipitaten von stabilen polyklonalen Zelllinien, welche Wild-Typ GLIS2 in niedrigen nahezu physiologischen Leveln beziehungsweise zwei weitere GLIS2-Varianten exprimieren, generiert. Interessanterweise konnten, entsprechend der zugrundeliegenden Hypothese, Hauptkomponenten der DDR-Signalwege wie PARP1, DNA-PKcs und RAD50 unter den Interaktoren nachgewiesen werden [16,105]. Die Daten legen somit eine potentielle Rolle von GLIS2 im Rahmen des DDR und der damit verbundenen Aufrechterhaltung genomischer Integrität nahe. Darüber hinaus wurden zahlreiche Proteine des ziliären Kompartiments identifiziert, was auf eine Lokalisation von GLIS2 im Bereich des Primärziliums hinweist.

2. Introduction

2.1. The kidney and its basic function

The kidney is a pairwise arranged organ which is located in the retroperitoneum of the human body [85]. The two kidneys receive 20% of the cardiac output, which is 10 to 50 times higher as compared to other organs in relation to their weight [89]. The main tasks of the kidneys are the secretion of toxic components, which are solved in the blood through the urine, and the regulation of the intravasal volume [62]. The kidneys of a healthy adult produce 180 l of primary urine per day [128]. Besides the elimination of toxic substances, the kidney has many other regulatory functions. The kidney is the main effector organ in regulating the volume, electrolyte and acid-base homeostasis, and arterial blood pressure [62]. Furthermore, it has endocrinological functions like the production of erythropoietin, and it converts a biologically inactive precursor of vitamin D in its active form, thereby regulating Ca^{2+} homeostasis, which has a crucial influence on bone mass [62]. Therefore, it becomes clear that the kidney performs pleiotropic functions for physiological homeostasis.

The functional subunit for urine production in the kidney is the nephron [62]. It starts with the glomerulus, which consists of convoluted arterial capillaries [120]. These capillaries have a fenestrated endothelium and are surrounded by a basement membrane [120]. On top of this basement membrane is a cell layer (visceral part of the Bowman's capsule) of a specialized cell type called podocytes which are interdigitating with each other by small food processes, thereby covering the whole capillary surface [120]. Together these three layers make up the glomerular filter which determines what kind of dissolved substances can get from the blood into the primary urine in the Bowmann´s space [120]. The Bowman's space is the beginning of the tubule system of the nephron. Here the ultrafiltrate of the blood (also called primary urine) enters the tubule system [62]. In the following segments of the tubule system, the primary urine is modified through reabsorption processes and secretion processes into the lumen of the tubule [62]. The tubular epithelial cells of the different segments have a specialized composition of transmembrane transport proteins and ion transporters to facilitate the reabsorption processes for the different substances in the primary urine, which need to be reabsorbed or secreted into the lumen of the tubule [62]. The different segments, starting from the Bowmann's space, are the proximal tubule, the thin descending limb, the thin ascending limb, the thick ascending limb of the loop of Henle, the distal tubule, and the collecting duct [62]. The collecting ducts of the single nephrons of one pyramid drain into one of the minor calyxes that unite to the major calyx merging into the ureter consecutively [85]. Tubular epithelial cells of all parts of the nephron share one common feature of great importance for the maintenance of the tissue architecture and function: They carry primary cilia on their apical surface [104]. Cilia are sensory organelles that project into the lumen of the tubules [104]. These cilia play essential roles during development and are essential for tissue homeostasis in the kidney.

2.2. Architecture of the primary cilium

Cilia are specialized sensory cell organelles [104]. Structurally, they are small antennae-like pullouts of the plasma membrane, which are stabilized by a microtubule scaffold [104]. Each cilium is anchored with the basal body, which is a modified mother centriole [104]. The basal body itself is anchored to the plasma membrane by transition fibers. There are two major types of cilia: Motile cilia are often organized in bundles of multiple cilia (e.g., on respiratory epithelial cells where motile cilia cover the apical surface of the cell, which is orientated to the lumen and exhibit a metachronous movement for efficient propulsion of mucus), but there are also cell types which have only one motile cilium like, e.g., sperm cells [117]. In both cases, motile cilia mainly carry out mechanic functions like cell motility or propulsion of extracellular fluids [110]. Non-motile cilia are present singularly on eukaryotic cells and are typically referred to as primary or sensory cilia [117]. The primary cilium is formed once a cell has exited the cell cycle (G0/G1 phase), at a time when the centrosomes are not needed as a pole for the mitotic spindle during mitosis [50,109,130]. The major architectonical difference between motile and non-motile cilia lies within the composition of their axoneme [109]. The axoneme of motile cilia consists of nine radially arranged microtubule doublets and one central microtubule doublet (9+2 structure), whereas primary cilia lack the central microtubule pair (9+0 structure) [109]. Primary cilia are also lacking the inner and outer dynein arm. Notably, the protein composition of the ciliary compartment and the ciliary membrane is different from other subcellular compartments and is established by a permeability barrier called the ciliary gate at the ciliary base, which strictly regulates the entry and exit of proteins [9,44]. The ciliary gate consists of the transition fibers at the transition zone whose major structural key components are so-called Y-links which project from the ciliary axoneme close to the ciliary base towards the plasma membrane [44]. From the mother centriole to the ciliary gate, a third microtubule (so-called C-tubule) abuts on each of the nine microtubule doublets [104]. The transport of membrane proteins is facilitated by lateral transport through the ciliary gate and is thought to be regulated by members of the septin protein family [67,109].

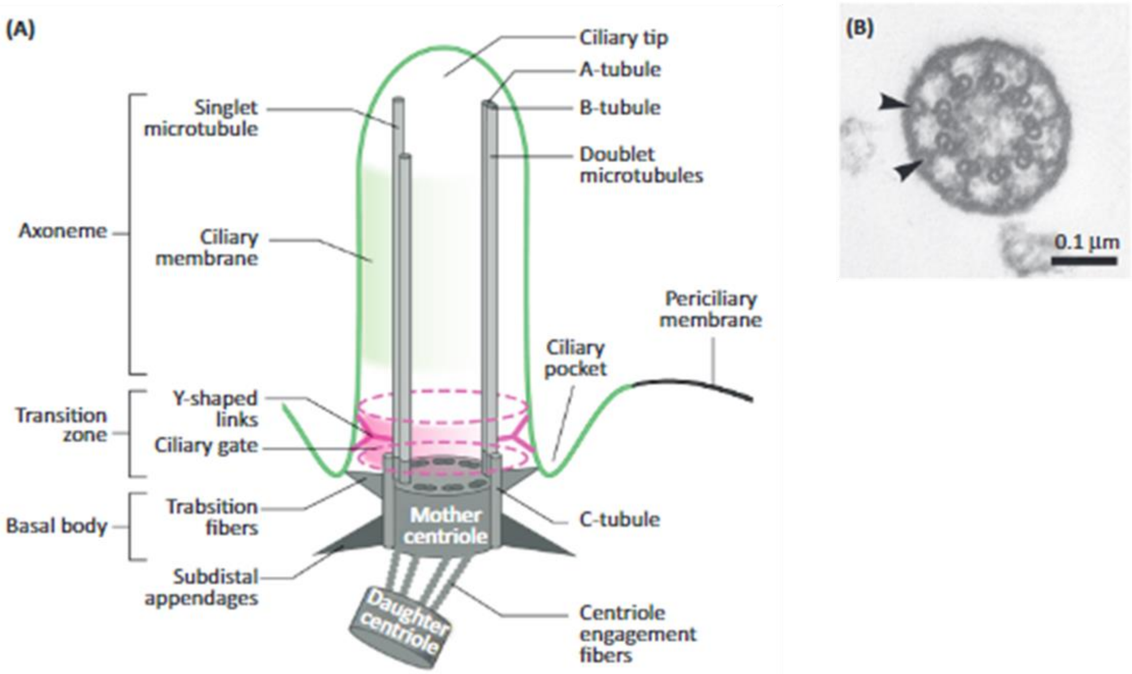

Fig. 1: **The primary cilium** (A) A simplified schematic presentation of the ultrastructure of the primary cilium (components are not true to scale). (B) A transmission electron micrograph of photoreceptor connecting cilium. Note the 9+0 structure consisting of nine microtubule doublets. Arrowheads pointing on Y-linkers which are part of the transition zone. Figure from Malicki, J.J. and C.A. Johnson, (2017) [104].

The transport inside of the primary cilium is mediated by IFT (intraflagellar transport) protein complexes which are coupled to kinesin or dynein motor proteins which facilitate the movement of the IFT complexes along the microtubules of the ciliary axoneme [71,109]. IFT-B complexes are coupled to kinesin motor proteins for anterograde transport towards the ciliary tip, whereas IFT-A complexes are coupled to dynein motor proteins for retrograde transport back to the ciliary base [71,109].

2.3. Function of the primary cilium

The main task of primary cilia is to sense extracellular signals and transmit those towards the cell body [104]. In this manner, the primary cilium is to be understood as a signaling hub for the extracellular environment and its stimuli [146]. The unique composition of the ciliary membrane facilitates these diverse sensory tasks as it inherits a broad spectrum of different receptors and the downstream components of the related signaling pathways [45]. Important pathways related to cilia are, for example, Wnt signaling, Notch signaling, Hedgehog signaling, Hippo signaling, and mammalian target-of-rapamycin (mTOR) signaling [117].

Hedgehog (HH) signaling plays an essential role in embryonic development and stem cell maintenance and requires the primary cilium as a signaling compartment [68,92,117]. When Hh binds its receptor patched (PTCH), this complex moves out of the cilium and allows smoothened (SMO) (a transmembrane protein) and kinesin family member 7 (KIF7) together with the Gli transcription factors (Gli1-3) to enter the ciliary compartment [27,117,129]. SMO and KIF7 inhibit suppressor of fused (SUFU), which terminates the inhibition of Gli by SUFU, thereby promoting its activation (GliA) and its transport out of the ciliary compartment towards the nucleus where it can perform its functions as a transcription factor [43,117,127,142].

Wnt signaling regulates cell migration, planar cell polarity, and organogenesis [117]. Wnt, a glycoprotein, binds to its transmembrane receptor frizzled thereby inducing the recruitment of the degradation complex of β-catenin consisting of Axin, adenomatous polyposis coli (APC), casein kinase 1 (CK1), and glycogen synthase kinase 3β (GSK-3β) [15,33,43,47,117]. This leads to β-catenin escaping this complex and its consecutive translocation to the nucleus to perform its transcriptional functions [117]. This signaling cascade is modified by the primary cilium, e.g., through mechanical stimuli sensed by the primary cilium via mechanosensitive ion channels [117].

mTOR signaling regulates cell growth, survival, proliferation, and cell cycle progression [117]. An important regulation of mTOR signaling consists in the flow-induced bending of the primary cilium (e.g., in the kidney), which activates liver kinase B1 (LKB1) and induces its transport from the ciliary compartment towards the basal body where it phosphorylates and activates AMP-activated protein kinase (AMPK) [17,117]. AMPK, in turn, phosphorylates tuberin (TSC-2), which together with hamartin (TSC-1) inhibits ras homolog enriched in the brain (RHEB) [117]. This blocks the activation of mTOR through RHEB [117]. This mechanism is thought to be crucial for cell size control of renal epithelial cells and their homeostasis, which is important for preventing cyst growth in the kidneys [13,17,117].

Different hypotheses have been formulated concerning the way primary cilia are integrated into renal physiology. One of those hypotheses states that receptors of the G_{olf} receptor family which are found within the membrane of primary cilia might sense extracellular levels of different extracellular substances surrounding tubule epithelial cells [118]. Another interesting hypothesis concerning the function of primary cilia in kidney physiology states that primary cilia might be involved in an auto-regulative control loop that adjusts the sodium resorption of distinct nephron segments (mainly of the collecting duct) to the flow rate of the respective nephron and,therefore its glomerular filtration rate (GFR) [34-36,118].

2.4. Impaired function of ciliary proteins results in ciliopathies

Ciliopathies are defined as a group of genetic diseases caused by impaired structure or function of primary cilia with consecutive characteristic phenotypical abnormalities [60].

The following introduction on ciliopathies will focus on the subgroup of ciliopathies associated with a dysfunction of primary cilia [60]. As the function or structure of a widely expressed cell organelle is impaired in ciliopathies, the function and architecture of many different tissues can be affected [60]. Ciliopathies exhibit a broad phenotypic spectrum which includes retinitis pigmentosa, cystic kidney disease, *situs inversus*, intellectual disability, hypoplasia of the corpus callosum, Dandy-Walker malformation, hepatic disease, obesity, polydactyly, craniofacial malformations, skeletal malformations, deafness, and anosmia [60]. A large subgroup of ciliopathies, however, shares the phenotypic feature of cystic kidney disease [60]. According to this feature, ciliopathies can be classified as renal ciliopathies and non-renal ciliopathies [6]. Among renal ciliopathies are autosomal dominant polycystic kidney disease (ADPKD; OMIM 173900 (*PKD1*), OMIM 613095 (*PKD2*)), autosomal recessive polycystic kidney disease (ARPKD; OMIM 263200), nephronophthisis (NPHP), Senior-Løken Syndrome (SLSN; OMIM 266900), Joubert Syndrome (JBTS; OMIM 213300), Bardet Biedl Syndrome (BBS; OMIM 615593), Meckel Gruber Syndrome (MKS; OMIM 249000), Oro-facial-digital Syndrome (OFD; OMIM 311200), Cranioectodermal Dysplasia (CED; OMIM 218330), Short Rib Polydactyly (SRP; OMIM 631091) and Jeune Asphyxiating Thoracic Dystrophy (JATD; OMIM 208500) [6]. There is genetic and phenotypic overlap between these syndromes, and the genotype-phenotype-correlation and the underlying genetics are complex as different mutations of the same type (e.g., missense mutation) in the same gene can cause different syndromes [126]. For many ciliopathies, the complex connection between the genotype and the resulting phenotype remains unknown [126].

2.4.1. Renal ciliopathies: ADPKD and ARPKD

The most common type of renal ciliopathies is ADPKD, with a prevalence of 1 in 1000 to 1500 [28,91,148]. In 85% of the cases, mutations in the *PKD1* gene encoding for polycystin-1 (PC-1) and in 15% of the cases mutations in the *PKD2* gene encoding for polycystin-2 (PC-2) are causative for ADPKD [29]. The pathophysiology of this disease is not yet completely understood [28]. PC-1 and PC-2 are transmembrane proteins localized in the ciliary membrane [69,111]. One current hypothesis is that loss PC-1 or PC-2 leads to low intracellular calcium levels leading to a decreased inhibition of adenylate cyclase 6 (AD6) which in turn leads to increased cAMP levels, protein kinase A (PKA) activation, and consecutive activation of Wnt signaling and mTOR signaling which mediate uncontrolled proliferation, loss of planar cell polarity and fluid secretion (through the cystic fibrosis transmembrane conductance regulator (CFTR) chloride channel) [28]. These alterations lead to massive cyst growth in the kidney and consecutive ESRD around the sixth decade [28]. Extra-renal manifestations of ADPKD include arterial hypertension, intracranial aneurysms, liver, and pancreatic cysts, abdominal hernias, and lesions of cardiac valves [11,20,21,28,63]. In contrast, ARPKD has a prevalence of 1 in 20000 and is caused by mutations in the *PKHD1* gene, which encodes for fibrocystin [53,147]. Patients with ARPKD often get diagnosed *in utero* [52]. The kidney dysfunction leads to the development of a Potter sequence with lung hypoplasia [77]. Almost all ARPKD patients exhibit liver fibrosis with portal hypertension [14].

2.4.2. Nephronophthisis

Nephronophthisis (NPH) is the most common genetically determined cause of end-stage renal disease in early childhood [99]. Kidney failure is due to the development of excessive fibrosis and cysts at the corticomedullary border in the kidneys of these patients, which replaces the functional kidney tissue [99]. As there is currently no causal therapy available, these patients typically are dialyzed until they receive a donor kidney for transplantation [99]. Today mutations in ≥20 different genes have been associated with the development of the clinical phenotype of NPH [99]. A feature that all the renal ciliopathy-associated genes (ADPKD, ARPKD, and NPH) are thought to have in common is that their respective gene products all localize to the primary cilium [99]. That is the reason why NPH is classified as a ciliopathy [99]. NPH is inherited in an autosomal-recessive way [99]. Juvenile NPH has a median onset of end-stage renal disease (ESRD) at the age of about 13 (1 year for the infantile NPH and 19 years for the adolescent NPH) [99]. The renal phenotype of NPH is morphologically characterized by cysts at the corticomedullary border, renal fibrosis, and mild size reduction of the kidneys [99]. The clinical presentation consists of a concentration defect with polydipsia and polyuria, impaired sodium reabsorption from the primary urine resulting in hypovolemia and hyponatremia, chronic kidney disease, and proteinuria [99]. The NPH phenotype is also associated with extra-renal manifestations affecting organs like eye, liver, the central nervous system (CNS), heart, and bone [99]. The juvenile NPH phenotype is mainly associated with retinal degeneration, cerebellar vermis aplasia, gaze palsy, liver fibrosis, and skeletal defects [99]. There are genetically and phenotypically overlapping NPHP-related ciliopathies like SLS, JS, and BBS [99]. Among all cases of NPH, about 30% are caused by mutations in known NPHP genes, while in 70%, the pathogenetic mutation is still unknown [137]. In the at hand thesis, we focused on *NPHP7*, which encodes for GLIS2 [7]. This is a relatively rare subtype of NPH and is described in only very few families [7]. In addition, a phenotypically clear knock-out mouse model was published in 2007 by Attanasio *et al.,* which showed a lack of GLIS2 to be causative for an NPH-phenotype [7]. However, the pathogenetic mechanisms responsible for the development of NPH in the case of GLIS2 deficiency are largely unknown. In particular, the nuclear functions of GLIS2, which might contribute to the development of NPH, are not yet understood, although its nuclear localization is proven [145].

2.4.3. *NPHP7* encodes for GLIS2

Mutations in *GLIS2* in humans result in the clinical phenotype of juvenile NPH [99]. *GLIS2* was first identified to be causative for an NPH phenotype in a distinct patient cohort by Attanasio *et al.* in 2007 [7]. Three patient mutations are described so far [4,7]. The first one is a missense point mutation (c.523T>C→C175R) discovered in a family from Turkey, and the second one is a point mutation destroying a splice donor site (c.775+1G>T) right at the beginning of intron five of the GLIS2 gene discovered in a Canadian Oji-Cree kindred with high grade of consanguinity [7,56]. The third mutation was described in a case report from 2021 in a consanguineous Omani family [4]. The mutation is an in-frame deletion of five amino acids (c.562_576delCATGTCAACGATTAC; p.His188_Tyr192del), thereby destroying the first zinc finger motif [4]. In the frame of the publication by Attanasio *et al.* of 2007, the phenotype of a *Glis2* knock-out mouse line was also characterized [7]. This knock-out mouse line exhibits a classical NPH phenotype with excessive fibrosis of the kidney and cysts at the corticomedullary border and on the molecular level upregulation of genes involved in apoptosis and fibrosis [7].

Gli-similar family zinc finger 2 (GLIS2) is a DNA-binding Krüppel-like transcription factor that mainly localizes to the nucleus [145]. Additional subcellular localizations of GLIS2 like the primary cilium are not yet clearly proven (further discussed in section 5.4.) [7].

The *GLIS2* gene is located on chromosome 16 and encodes for a protein that consists of 524 amino acids that form five zinc finger domains facilitating DNA-binding and thus its transcriptional activator and repressor functions [152]. The first three zinc finger domains are essential for the nuclear import of GLIS2 [145]. GLIS2 gets cleaved between the fourth and the fifth zinc finger domain [66]. This cleavage is induced by the interaction with catenin delta 1 (CTNND1) [66]. GLIS2 binds to the so-called Glis-binding sequence (GlisBS) ((G/C)TGGGGGGT(A/C)) and the Gli-binding site (GBS) (TGGGTGGTC) with the GlisBS, e.g., found in the murine insulin 2 promotor, thereby negatively regulating insulin 2 expression [145].

The development of fibrosis in the context of loss of GLIS2 seems to be dependent on epithelial to mesenchymal transition (EMT) as the knock-out mouse model revealed an upregulation of a cluster of genes involved in EMT like Slug (SNAI1), Snail (SNAI2), and TGFβ [7]. A more recent publication from 2016 by Lu *et al.* also uncovered that

GLIS2 deficient cells exhibit elevated levels of phosphorylated histone H2AX (γH2AX), which is a marker for activated DNA damage response [98]. This was the first time that loss of GLIS2 was linked to an activation of DNA damage response (DDR) signaling. This connection was further confirmed by laser ablation experiments of Slaats et al. (unpublished data), which have shown overexpressed GFP.GLIS2 to be recruited to nuclear areas of laser-induced DNA double-strand breaks [49]. GLIS2 also acts as a repressor of Hedgehog signaling [94]. Nevertheless, much about GLIS2 physiology and the pathogenetic mechanisms occurring in NPH type 7 is still unknown.

2.5. Cilia and DNA damage response

Since 2012, DNA damage (DD) and DD response (DDR) signaling have been implicated with genes encoding for ciliopathy proteins (Chaki *et al.* Cell, 2012) [19]. In the field of primary cilia and ciliopathy research, the connection between primary cilia and DDR signaling and the role of impaired DDR signaling as a potential main-contributor to the pathogenesis of ciliopathies – especially of NPH – gets more in the focus of interest as genetic studies identified NPH-causing genes with function in DD repair and DDR signaling [19]. This section will give a brief overview of DDR signaling and DNA repair mechanisms. The eukaryotic cell disposes over a set of signaling pathways that coordinate the recognition of DNA damage with cellular processes like DNA repair, apoptosis, cell cycle progression, or cellular senescence [25]. These pathways are collectively grouped under the term DNA damage response [25]. Different genotoxic influences can cause different types of DNA lesions like DNA single-strand breaks (SSBs), DNA double-strand breaks (DSBs), and lesions of single bases, which in turn lead to the initiation of specific signaling cascades [16,25]. Dependent on the severity and the amount of DNA damage, different strategies are applied, which encompass the direct repair, the pause of cell cycle progression, and cellular programs like senescence or apoptosis [25]. SSBs are initially recognized mainly by poly (ADP-ribose) polymerase 1 (PARP1) but also by PARP2 [125]. SSBs can also be recognized by replication protein A (RPA), especially in the context of replication stress with stalled replication forks which can lead to SSBs or DSBs [16]. DSBs can also be recognized by PARP1 like SSBs [25]. PARylated PARP1, in turn, serves as a platform for the heterotrimeric MRN complex consisting of meiotic recombination 11 (MRE11), DNA repair protein RAD50, and Nijmegen breakage syndrome 1 (NBS1) [25]. This complex leads to recruitment and activation of ataxia telangiectasia mutated (ATM) kinase which is the central kinase of this pathway [16,39]. ATM also activates p53, a central downstream factor, which leads to cell cycle arrest, DNA repair, and potentially to senescence or apoptosis [16,150].

Seven NPH-proteins have been already linked to DDR signaling, and a pathophysiologic contribution of impaired DDR signaling to NPH has been hypothesized [3,19,24,98,102,133]. These proteins are centrosomal protein of 290 kDa (CEP290; NPHP6), Gli-similar family zinc finger 2 (GLIS2; NPHP7), NEK8 (NPHP9), serologically defined colon cancer antigen 8 (SDCCAG8; NPHP10), zinc finger protein 423 (ZNF423; NPHP14), centrosomal protein of 164 kDa (CEP164; NPHP15) and mitogen-activated protein kinase binding protein 1 (MAPKBP1; NPHP20). The first NPH proteins which were linked to functions in DDR signaling in the publication of Chaki *et al.* in 2012 were ZNF423 (NPHP14) and CEP164 (NPHP15) [19]. The authors postulated that tissues that are mainly affected in these NPH subtypes and NPHP-related ciliopathies (NPHP-RC) like kidney, liver, and retina are affected because they have to cope with significant genotoxic factors [19]. The kidneys and the liver are confronted with a wide spectrum of substances that should be eliminated and excreted by the human body, and the retina is confronted with UV light [19]. Further evidence for this hypothesis can be seen in the phenotypic overlap of NPH and NPHP-RC and diseases caused by mutations in genes for DDR components like Seckel syndrome caused by mutations in the ATR gene, amongst others, which presents phenotypic features like microcephaly with mental retardation, facial dysmorphism and growth defects [25,78]. Another example is progressive cerebellar degeneration which can be caused by mutations in the MRE11 gene [19]. MRE11 is part of the MRN complex, which is a central component of the ATM pathway in response to DSBs [16]. These patients show cerebellar vermis aplasia, which is also a common phenotypic feature of NPHP-RC [19].

The reciprocal influence between ciliary and nuclear processes becomes clear while looking at the process of ciliogenesis and ciliary disassembly in coordination with the cell cycle progression, which was already described in section 2.2. In response to cell cycle progression (entering of S-phase), this information is transmitted to the primary cilium, and ciliary disassembly is initiated as the centriole is needed for spindle pole formation during mitosis [109,146]. Vice versa, signaling cascades starting in the ciliary compartment in response to external stimuli can result in transcriptional changes in the nucleus, like in the case of mTOR signaling, which is decisively influenced by the primary cilium and regulates, e.g., cell proliferation through cell cycle regulation [117]. The complex interplay between the two compartments is not fully understood yet. An important structure for the understanding of this complex interplay is the centriole which links both compartments to each other [75]. Interestingly, a group of proteins involved in DDR and cell cycle regulation are also found at the centriole at the ciliary base besides their main localization in the nucleus. Among these proteins are ATM, ATR, ATRIP, CHK1, CHK2, cyclin-dependent kinase 1 (CDK1), CDK4 and cyclin A [37,42,90,116,141,144,153]. This leads to the hypothesis that the centriole functions as a signaling hub between these two compartments [5]. However, the underlying pathways are poorly understood. It is also not known if one of these proteins shuttles between its two pools at the centriole and in the nucleus and to which extent this occurs.

2.6. Hypothesis and aims

NPH is an autosomal-recessive inherited renal disorder that is characterized by excessive fibrosis, cysts at the corticomedullary border, and size reduction of the kidneys, all resulting in ESRD in early childhood [7]. NPH is classified as a ciliopathy as all gene products of the disease-causing genes (≥20) are localizing to the primary cilium and are associated with impaired ciliary function in case of mutation. Little is known about the pathogenesis of NPH so far but recently 7of the NPH proteins have been implicated in the DNA damage response, which led to the hypothesis that these proteins play an important role in genome maintenance and for a proper DNA damage response required to preserve tissue homeostasis in the kidney. GLIS2 is a DNA-binding Krüppel-like transcription factor that mainly localizes to the nucleus and was first identified to be causative for an NPH phenotype (NPHP7) in a distinct patient cohort by Attanasio *et al.* in 2007 [7,145].

The primary aim of the at-hand thesis was to gain a better understanding of the pathophysiologic mechanisms underlying the development of nephronophthisis caused by *GLIS2* mutations and to uncover GLIS2 functions by characterizing GLIS2 interacting proteins. One of the objectives was to create a GLIS2 interactome. Therefore, we will pursue antibody-based approaches, including the validation of an existing commercial anti-hGLIS2-antibody and the generation of a homemade monoclonal anti-mGLIS2-antibody by hybridoma culture. In parallel, we will pursue cell line-based approaches, which will encompass the generation of an IMCD3 FLAG-GFP-knock-in GLIS2 cell line using the CRISPR/Cas9 genome editing system and a HEK293T GFP.P2A.3xFLAG GLIS2 cell line using the TALEN genome editing system. These biochemical tools will be used to precipitate GLIS2 together with protein interactors which will be measured by MS/MS. Additionally, with those antibodies and cell lines, we aim to visualize the subcellular localization of GLIS2. Taken together, we hope to learn more about the subcellular localization of GLIS2 and to obtain the first interactome of GLIS2 to characterize GLIS2 functions further. Our findings will contribute to the understanding of how GLIS2 plays an important role in genome maintenance and thereby preserving tissue homeostasis in the kidney.

3. Material and Methods

3.1. Cell culture

The whole work with eukaryotic cells was done under sterile conditions under a hood with a continuous airflow to prevent particles from entering the space inside the hood [8]. As mammalian cell lines HEK 293T, human U2OS, mouse IMCD3, and HeLa Kyoto were cultured. The cells were cultured in 10 ml DMEM (only mouse IMCD3 cells were cultured in DMEM F-12 + GlutaMAX) with 10% fetal bovine serum in plastic dishes with a diameter of 10 cm in an incubator at 37°C and 5% CO_2. For passaging of the cells, the medium was aspirated with a vacuum device. Then the cells were washed with 1x PBS (10 ml). This step is to eliminate excess BSA, which would inhibit the enzymatic activity of trypsin (1 ml) which is used to detach the cells from the bottom of the dish [58]. After incubation at 37°C for 3-10 min (depending on the strength of attachment) medium was added to the dish to stop the enzymatic activity of trypsin and to resuspend the cells and divide them onto new dishes with a final culturing volume of again 10 ml.

3.1.1. Materials for cell culture

Material	**Manufacturer**
Dulbecco's Modified Eagle's Medium (DMEM) with 4.5 g/l D-Glucose, Pyruvate, GlutaMAX + 10% fetal bovine serum	Life technologies (31966-021) Life technologies
Dulbecco's Modified Eagle's Medium Nutrient Mixture F-12 with 15 mM HEPES, $NaHCO_3$ + 10% fetal bovine serum + GlutaMAX (100x)	Sigma (D6421-500ML) Life technologies Life technologies
PBS Buffer: 136 mM NaCl, 2.7 mM KCl 6.25 mM Na_2HPO_3, 1.5 nM KH_2PO_3, pH 7.4	Nephrolab Roth Merck
Trypsin-EDTA (0.25%)	Thermo Fisher
HEK 293T (human embryonic kidney)	ATCC
Human U2OS (human bone osteosarcoma)	ATCC
HeLa Kyoto (human cervix adenocarcinoma)	ATCC
Mouse IMCD3 (mouse inner medullary collecting duct)	ATCC
Cell culture dishes (10 cm plates, 6-well, 12-well, 24-well, 96-	Corning

well)	
Stripetts (5 ml, 10 ml, 30 ml)	Corning
Sterile pipet tips (10 µl, 200 µl, 1000 µl)	Starlab

3.2. Transfection

3.2.1. Calcium-Chloride Transfection

Transfection describes the process of importing DNA into cells [22]. This process is used in a biotechnical context to import plasmids that contain a certain cDNA in mammalian cells to make them produce the proteins which are encoded by the cDNA [82]. For transfection with $CaCl_2$, the plasmid (10 µg) which is supposed to be transfected was pipetted together with 500 µl $CaCl_2$ in one tube. This tube was put on the vortexer with the lid open. Then 500 µl 2x HEPS buffer was added dropwise while vortexing. The HEPS buffer induces $CaCl_2$ to form crystals to which the plasmid is attached [22]. After adding this mix to the cells (circa 50% confluency for $CaCl_2$ transfection), they start ingesting the crystals in the intercellular space via endocytosis and thus incorporate the plasmid in their cell body [23]. This reaction was then stopped after 6 to 8 hours by aspiration of the old medium and the addition of a new medium.

3.2.2. Materials for transfection with $CaCl_2$

Material	Manufacturer
$CaCl_2$	Roth
2x HEPS buffer: 50 mM HEPES (4-(2-hydroxyethyl)-1-piperazineethanesulfonic acid), 280 mM NaCl, 10mM KCl, 12 mM dextrose 1.5 mM Na_2HPO_3, pH 7,09, sterile-filtered	Nephrolab Roth Roth Sigma
Tubes (1.5 ml)	Eppendorf

3.2.3. Transfection with Lipofectamine

This transfection method is based on the formation of lipid vesicles that incorporate the plasmid and can fuse with the cell membrane [40]. Lipofectamine facilitates this vesicle formation [40]. For a 6-well, two mixes were made. Both contained 200 µl Optimem, and one contained 7 µl lipofectamine 2000, and the other one contained the desired amount of plasmid. Then the two mixes were incubated for 20 min at room temperature together. The initial mixing should be done without pipetting and only by flicking the tube gently. In this incubation step, lipid vesicle formation takes place [40]. After this incubation step, the whole mixture was added to the cells. The cells should have a confluency of above 60% because lipofectamine has toxic effects on the cells. This reaction has not to be stopped, and the cells were processed the next day.

3.2.4. Materials for transfection with Lipofectamine

Material	Manufacturer
Lipofectamine 2000	Invitrogen
Optimem	Invitrogen

3.3. siRNA knock-down

RNA interference is a principle used by eukaryotic cells to regulate protein expression on the mRNA level by so-called small interfering RNAs which can target a specific mRNA species [32]. In the physiologic context, a short hairpin RNA is produced, which gets cleaved into small interfering RNAs by ribonucleases like Dicer or Drosha [32]. The resulting double-stranded siRNAs are separated into single strands, and the formation of an RNA-induced silencing complex (RISC) is induced [32]. This RISC complex facilitates the hybridization between its single-stranded siRNA molecule and the complementary mRNA, which is subsequently degraded [32]. Thus, the mRNA cannot be translated into the respective protein, which results in a knock-down of this protein [32]. In the biotechnical context, mammalian cells are transfected with siRNA using lipofectamine RNAimax [82].

3.3.1. siRNAs used in this work

Gene	Name	Target sequence	Manufacturer
GLIS2	siGlis2	5’CCACUGCGCUAUUUGGAUG 3’; 5’CCAAGCAGCUGGUGUGUCG 3‘; 5‘ACAAGUGCCUCUCGCCAGA 3‘; 5‘CCGAGAAGGAUGCGGGUA 3‘	Dharmacon
Control	siCtrl	5’UGGUUUACAUGUC GACUAA 3’; 5’UGGUUUACAUGUU GUGUGA 3’; 5’UGGUUUACAUGUU	Dharmacon

		UUCUGA 3'; 5'UGGUUUACAUGUU UUCCUA 3',	

3.4. Harvesting and lysis of cells

Cells were harvested by aspiration of the medium and addition of 1x PBS (4°C) per one 10 cm dish. Then they were scraped off the bottom by a cell scraper. The cell suspension was collected with a stripette and collected in a tube or a falcon and then centrifuged at 1000 rpm at 4°C for 5 min. The supernatant was aspirated, and the remaining cell pellet could be lysed by adding a lysis buffer like modified RIPA buffer or could be snap-frozen by putting the tube/falcon in liquid nitrogen and stored at -80°C to process these cells for an experiment at a later time point.

3.4.1. Materials for harvesting and lysis of cells

Material	**Manufacturer**
PBS	
2x Laemmli buffer: 100 mM Tris, 20% glycerol, 4% SDS, 0,2% bromphenol blue, 100 mM dithiothreitol, pH 6,8	Nephrolab Roth Sigma
Modified RIPA buffer: 1% Tergitol-type NP-40 (nonyl phenoxypolyethoxylethanol), 0.25% sodium deoxycholate, 50 mM Tris-HCl, 150 mM NaCl, 1 mM EDTA, 1 mM NaF	Nephrolab Sigma Roth Sigma
PIM	Roche
PMSF (57 mM)	Sigma
Na_3VO_4 (100 mM)	Sigma
Falcons (15 ml, 50 ml)	Greiner bio-one
Centrifuge	Eppendorf
Cell scraper	Corning

3.5. Immunoprecipitation

Immunoprecipitation (IP) is a method to enrich a specific protein from a whole cell lysate by its interaction with an antibody, which targets a specific epitope of this protein [12]. The antibody is coupled to particles that are called beads which have a high density [12]. This allows the separation of the bead-antibody-protein complex from the rest of the cell lysate [12].

First, 500 µl modified RIPA buffer (+ 400µl/10ml protease inhibitor mix (with EDTA) and 200 µl/10 ml Na_3VO_4 (2 mM final concentration)) was added to the cell pellet (of a confluent 10 cm dish). The cell pellet was dissolved in the buffer by pipetting up and down to ensure sufficient lysis of all cells. The suspension was incubated for 15 min on ice. Then the lysate was sonicated with 20 pulses (10% power and 0.1 s on and 0.9 s off) to disrupt also the nuclear membrane, shear the DNA, and bring the nuclear proteins in solution [101]. This step is essential for two reasons. First, we were mainly working with GLIS2, which mainly localizes to the nucleus, and second, the modified RIPA buffer is one of the harsher lysis buffers but is not sufficient to disrupt all nuclear membranes without additional sonication [145]. Next, the lysate was centrifuged at 14000 rpm at 4°C for 15 min. Thereafter the supernatant was saved, which contains the proteins of the cell. A small amount (50 µl) of the lysate was separated and boiled with 2xLaemmli buffer (50 µl) at 95°C to load this together with the immunoprecipitation sample to judge the efficiency of the immunoprecipitation. To the rest of the lysate 50 µl of antibody-coated sepharose beads (in this case with an anti-FLAG-(M2)-antibody) was added and incubated on an overhead shaker overnight at 4°C (in a cold room). The next day the beads were washed three times with 700 µl modified RIPA buffer. One washing step consists of centrifugation at 4000 rpm at 4°C for 3 min, aspiration of the supernatant, adding of fresh modified RIPA buffer, and 5 min incubation on the overhead shaker at 4°C. After the last washing step, the beads were either boiled at 95°C with 50 µl 2xLaemmli buffer to analyze the sample by western blot or incubated with 50 µl of an elution buffer containing 2 mg/ml 3xFLAG-peptide in 1xPBS for one hour on ice. The elution variant was used to keep the native protein structure of the immunoprecipitated protein and to detach it from the beads without denaturation like it is required for mass spectrometry measurements to detect, e.g., protein interactors of the immunoprecipitated protein [139]. In this case, the eluate was saved and incubated with dithiothreitol (DTT) (5 mM final concentration) for 30min at 55°C to reduce disulfide bonds and with chloroacetamide (CAA) (40 mM final concentration) for 30min at room temperature in the dark for alkylation to prevent further post-translational modifications [55]. Finally, the samples were stored at -20°C and processed by the CECAD proteomics facility to analyze the sample by mass spectrometry.

3.5.1. Materials for immunoprecipitation

Material	**Manufacturer**
FLAG(M2)-beads	bimake.com (B23102)
Protein G-beads	GE Healthcare (17-0618-01)

3xFLAG-peptide	Sigma (F4799-4MG)
Dithiothreitol	Roth
Chloroacetamide	Sigma
Sonicator	Branson
Overhead shaker	

3.5.2. Nano-liquid-chromatography-(nLC)-MS/MS proteomic analysis of immunoprecipitation samples

After incubation with DTT and CAA, as described previously, each sample was incubated at RT overnight with trypsin and LysC for digestion of the proteins. Digestion was stopped by addition of 0.5% formic acid and further cleaned and desalted using stop-and-go extraction tips (Stagetips) [131]. Before MS/MS analysis, peptides were resuspended in 0.1% formic acid, and peptides were fractionated by nLC with a 1-hour gradient and a binary buffer system. Samples were finally measured using a quardrupole-orbitrap based QExacutive mass spectrometer (Thermo Scientific) [107].

3.5.3. Bioinformatic analysis of raw mass spectrometry data

After the mass spectrometry measurement, the raw mass spectrometry data was quantified and normalized with MaxQuant software [31]. The protein group files (output of MaxQuant) were further analyzed with Perseus version 1.5.5.3 [30,143]. Reverse hits, contaminants as well as proteins identified by site only were removed from the search results. LFQ expression values were logarithmized ($\log_2$). Replacement of missing values from normal distribution was performed with a downshift of 1.8 and a width of 0.3. Finally, significant interactors of the immunoprecipitated fusion protein of one of the cell lines were visualized in a half volcano plot by plotting the negative logarithmized p-value ($-\log_{10}$ (p-value)) of a single protein group against its logarithmized ($\log_2$) LFQ-value in the tagged cell line versus the control line (in this case HEK293T GFP.P2A.3xFLAG.GLIS2 TALEN lines versus the HEK293T GFP.P2A.3xFLAG TALEN control line). The bioinformatic analysis of raw mass spectrometry data was mainly done by Dr. rer. nat. Christian Frese, the head of the CECAD proteomics facility.

3.6. SDS-PAGE and Western blot

Western blot (WB) is one of the standard techniques in biological research to detect a protein, which was separated by its size from others before, by its specific interaction with an antibody [12]. First, one has to pour the SDS-PAGE to separate the proteins of a cell lysate by size. Therefore, the mix for the separating gel, which contains a variable percentage of acrylamide, was poured first in a special plastic cassette. The acrylamide polymerizes after the addition of TEMED and APS to Polyacrylamide [103]. The mix for the collecting gel was then poured on top of the separating gel and polymerized after 5 to 10 minutes with a comp in it to form slots for the loading of the probes afterward. The percentage of acrylamide that is added to the mix for the separating gel determines the density of the gel and thus how easily denatured, and negatively charged proteins diffuse through the polyacrylamide gel by electrophoresis [12]. Boiling of proteins at 95°C with 2xLaemmli buffer, which contains SDS, denatures and charges proteins negatively, which makes the electrophoresis mainly dependent on its protein weight. The cassette was put in an electrophoresis chamber, which was filled with running buffer. This contained glycine, which is mainly zwitterionic at a pH of 6.8 and is stabilized by Tris in this buffer [12]. The probe sinks in the slot because of the glycerol in the Laemmli buffer [103]. If a voltage is applied glycine in the running buffer on top of the probe runs behind the probe, and small chloride anions run in front of the probe [12]. Thus, the probe gets compressed, and all proteins of the probe enter the separation gel at the same time (70 V for 30 min for the collection gel) [12]. In the separation gel, the pH switches to 8.8, which makes glycine mainly charged negatively [12]. Thus, it gets stronger attracted by the anode and runs now in front of the proteins (at 25 mA for 90 min) [12]. This pH switch and the Tris-glycine-chloride-buffer system facilitate the precise electrophoretic separation of the proteins by their molecular weight [12]. After electrophoresis, the proteins were immobilized on a PVDF-membrane for the following detection of specific proteins with antibodies [54]. The proteins migrate out of the gel on the PVDF-membrane again by electrophoresis between two plates where a potential is applied (12 V for 53 min) [54]. The PVDF-membrane was activated for protein binding with methanol before the transfer, and a sheet of filter paper (transfer buffer-soaked) inhibits direct contact between the plates and gel and PVDF-membrane [54]. After the transfer, areas of the membrane that had not bound protein were prevented from binding antibodies in the future nonspecifically by blocking the membrane in 5% bovine serum albumin (BSA) (in protein wash buffer) for 60 min [103]. Then the membrane was washed three times 5 min in protein wash buffer to get rid of abundant BSA. The membrane was then incubated with the first antibody, which targets specifically the protein which should be detected in the end (in a 1:200-10.000 dilution (depends on the concentration of the antibody and its affinity to the antigen) in protein wash buffer for 1 hour at room temperature or 4°C overnight). After renewed washing (3x 5 min in protein wash buffer), the membrane was incubated with the secondary antibody, which specifically targets the Fc-region of the first antibody (in a 1:30.000 dilution in protein wash buffer) [12]. The Fc-region is identical for a specific antibody subclass from a specific species [74]. So one has to consider from which species the first antibody derives. The Fc-region of the secondary antibody is connected to an enzyme called horseradish peroxidase which facilitates the decomposition of luminol in the presence of hydrogen peroxide under emission of low-intensity light (425 nm) [12,79]. This signal was detected in a dark chamber with the Fusion Solo Chemoluminometer. The resulting digital picture of the detection pattern on the membrane was further processed using Fusion software.

3.6.1. Materials for SDS-PAGE and Western blot

Material	**Manufacturer**
Collecting-gel: 5% acrylamide 125 mM Tris (pH 6,8) 0,1% SDS 0,05% APS 0,1% TEMED	 Roth Sigma Sigma Bio-Rad Sigma
Separating-gel: 10% acrylamide 375 mM Tris, 0,1% SDS, 0,05% APS, 0,05% TEMED, pH 8,8	
Running buffer: 25 mM Tris (pH 8,3), 0,1% SDS, 192 mM glycine	 Roth
Transfer buffer: 25 mM Tris (pH 8,3), 0,1% SDS, 192 mM glycine, 20% methanol	 Roth
Wash buffer: 10 mM Tris (pH 7.5), 100 mM NaCl, 0.1% Tween-20	 Roth Merck
ECL (Enhanced Chemiluminescence): 100 mM Tris (pH 8,5), 2,5 mM luminol, 0,4 mM coumaric acid, 1.5% hydrogen peroxide (H_2O_2)	 Fluka Sigma Merck
Isopropanol	Roth
Gel cassettes	Invitrogen

BSA (Bovine serum albumine) (5%)	PAA Laboratories
PVDF Transfer Membranes	Millipore
Blotting paper	VWR
Molecular weight standard protein ladder	Thermo Fisher

3.6.2. Primary antibodies for Western blot

Antibody	Species	Dilution	Manufacturer	Order no.
Anti-GFP (B2)	Mouse monoclonal	1:5000	Santa Cruz	sc-9996
Anti-GFP	Rabbit polyclonal	1:1000	Santa Cruz	sc-8334
Anti-FLAG	Mouse monoclonal	1:10000	Sigma	F3165
Anti-FLAG	Rabbit polyclonal	1:5000	Sigma	F7425
Anti-hGlis2	Rabbit polyclonal	1:200	Atlas Antibodies	HPA056976
Anti-Actin	Mouse monoclonal	1:500	DSHB	JLA20-s
Anti-β-Tubulin	Mouse monoclonal	1:500	DSHB	E7

3.6.3. Secondary antibodies for Western blot

Antibody	Species	Coupled with	Dilution	Manufacturer	Order No.
Anti-mouse IgG (H+L)	Goat polyclonal	HRP	1:30000	Jackson ImmunoLab	115-035-003
Anti-rabbit IgG (H+L)	Goat polyclonal	HRP	1:30000	Jackson ImmunoLab	111-035-144

3.7. Immunofluorescence staining

The immunofluorescence (IF) staining is based on the recognition of specific epitopes of native protein in or on fixed cells by an antibody [38]. The cells were grown to a confluency of 60-80% on a coverslip in a 6- or 12-well, which depends on the size of the coverslip. After aspirating the medium, the cells were fixed (cross-linking of all proteins of the cells) by addition of 4% paraformaldehyde (PFA) for 15 min [38]. The cells were washed 3 times with PBS and then blocked with 5% normal donkey serum (at RT for one hour) to reduce nonspecific antibody binding to cell proteins [38]. The blocking solution also contains 0.1% Triton-X, which makes the cell membrane permeable for large proteins [38]. Thus, the proteins of the NDS and the antibodies which are used for the staining can enter the cell [38]. Next, the cells were incubated (at 4°C overnight) with the first antibody in blocking solution (normal dilution of 1:1000, depending and the concentration of the antibody and its affinity to its antigen), which targets a specific protein whose localization in the cell should be visualized. After an additional washing step (3x 5 min), the cells were incubated with the secondary antibody, which targets specifically the Fc-region of the first antibody and is coupled to a fluorophore (Cy3, Cy5, Alexa 488, etc.) [106]. Finally, the cells were rewashed three times for 5 min and mounted upside down on a slide with Prolong Diamont, which contains DAPI, which stains the nucleus (binds DNA) (emission maximum around 460 nm upon binding of double-stranded DNA) [115]. Imaging was done with a LSM710 Zeiss confocal microscope equipped with a 63x objective and by using Zen software.

3.7.1. Materials for immunofluorescence staining

Material	Manufacturer
PBS	Biochrom AG
PFA (Paraformaldehyde)	Sigma
Triton-X 100	Appli Chem
Normal donkey serum	Jackson
Mounting solution Prolong Diamont with DAPI	Invitrogen
LSM 710 confocal microscope	Zeiss

3.7.2. Primary antibodies used for immunofluorescence staining

Antibody	Species	Dilution	Manufacturer	Order no.
Anti-Acetylated Tubulin	Mouse monoclonal	1:1000	Sigma	T6793
Anti-hGlis2	Rabbit polyclonal	1:100	Atlas Antibodies	HPA056976
Anti-FLAG	Mouse monoclonal	1:1000	Sigma	F3165
Anti-FLAG	Rabbit polyclonal	1:1000	Sigma	F7425

3.7.3. Secondary antibodies used for immunofluorescence staining

Antibody	Species	Coupled with	Dilution	Manufacturer	Order no.
Anti-mouse IgG (H+L)	Donkey polyclonal	Cy3	1:500	Jackson ImmunoResearch	715-165-150
Anti-rabbit IgG (H+L)	Donkey polyclonal	Cy3	1:500	Jackson ImmunoResearch	711-165-152
Anti-mouse IgG (H+L)	Donkey polyclonal	Alexa 488	1:500	Jackson ImmunoResearch	715-545-150

3.8. Cloning of plasmids

3.8.1. Primers (ordered from IDT)

Target	Name	Sequence
Glis2	*mGlis2* mlu fp	5’ CCC GCG ACG CGT ATG CAC TCC TTG GAC GAG CC 3’
Glis2	*mGlis2* rev 1-360bp	5’ CCC GCG GCG GCC GCA AGT GGC TGG AAA TCC ACA 3’
GLIS2	*hGLIS2* 1 mlu fp	5’ CGC GGG ACGCGT ATG CAC TCC CTG GAC GAG CCG CTC GAC CTG 3’
GLIS2	hGlis2 *Bgl-2 rp	5' CGC GGG AGA TCT TCA GTT CAC CAC AGC CGG T 3'
GLIS2	hGlis2 intron5 *Bgl-2 rv	5' CGC GGG AGA TCT TCA GAA GAT ACC CAC GGG AAC 3'
GLIS2	hGlis2 122 *Bgl-2 rv	5' CGC GGG AGA TCT TTA GCG CAG TGG CTG GAA GTC 3'
	AAV CAGGS GFP-P2A-3xFLAG Gibson fp	5' GAG CTG TAC AAG GGA ACG CGG GGA TCT GGG GCC ACA AAT TTT TCA CT 3'
	AAV CAGGS GFP-P2A-FLAG-GFP-hGlis2 Gibson rp	5' TTG GCA GAG GGA AAA AGA TCA GAT CTT CAG TTC ACC ACA GCC GGT TTG AGC AGC A 3’
Glis2	*Glis2*_3HA_BamH1_fp	5‘ CCC GCG GGA TCC ATG CAC TCC TTA GAT GAG CCC CTC GAC CTA AAG 3‘
Glis2	*Glis2*_3HA_EcoRI_rp	5‘ CCC GCG GAA TTC CTG TGT

		GTG TTC ATT GGG GA 3‘
Glis2	*Glis2*_5HA_HindIII_fp	5‘ CCC GCG AAG CTT GGT GAT AGT CCC CTG CCC TG 3‘
Glis2	*Glis2*_5HA_HindIII_rp	5‘ CCC GCG AAG CTT GGT GGG AGG GCG TGT CAA AG 3‘
Glis2	h&mGlis2 457bp FW	5‘ CCC AAG GAC AAG TGC CTC TC 3‘
GFP	GFP 646/664 fsp	5‘ CGC GAT CAC ATG GTC CTG 3‘
Glis2	*mGlis2* Surveyor NRP2	5‘ TTG CAC TAG GGT GTC TGC AC 3‘
AAV locus	AAVS1 integration pcr HA-R 2f	5‘ TAT CCG CTC ACA ATT CCA CA 3‘
AAV locus	AAVS1 integration pcr HA-R 2r	5‘ GTG AGT TTG CCA AGC AGT CA 3‘
AAV locus	AAVS 1 locus	5‘ CGG AAC TCT GCC CTC TAA CG 3‘
GFP	eGFP-rsp	5‘ CGC CGT CCA GCT CGA CCA GG 3‘
GFP	GFP FP 1 seq	5‘ ATG GTG AGC AAG GGC GAG G 3‘
GFP	GFP FP 2 seq	5‘ GAC GGC AAC ATC CTG GGG 3‘
GFP	EGFP_C fw	5‘ CAT GGT CCT GCT GGA GTT CGT G 3‘

3.8.2. PCR

The polymerase chain reaction (PCR) was developed by Mullis *et al.* (1986) and is a biotechnical method to multiply a specific double-stranded DNA fragment *in vitro* [112]. It is based on the multiple repetitions of a cycle consisting of denaturation of the DNA fragment, annealing of the primers, which serve as the starting point for the polymerase in the next step, elongation of DNA fragments with a thermostable polymerase and again denaturation, etc. [46]. The following reagents are necessary for this reaction. The PCR was done in a thermocycler (Biorad).

Reagent	**End concentration**	**Volume**
NEB Q5 Buffer	1x	5 µl
NEB Q5 Enhancer	1x	5 µl

NEB Q5 Hot Start	0,02 U/µl	0,25 µl
dNTP	0.2 mM	0,2 µl
Forward Primer	0.2 µM	0,5 µl
Reverse Primer	0.2 µM	0,5 µl
DNA template	depends on concentration	depends on concentration
H_2O	-	ad 25 µl

Step	**Temperature**	**Duration**
(1) Denaturation	98°C	30 s
(2) Denaturation	98°C	30 s
(3) Annealing	Depends on primer (3°C above the lower Tm (melting temperature) of both primers)	20 s
(4) Elongation	72°C	10 s per kb for simple and 40 s per kb for complex templates
Repetition of steps 2-4 34 times		
(5) Final extension	72°C	2 min
(6) Cooling	12°C	Forever

After the PCR, the amplified DNA fragments were digested with two different restriction enzymes, which prepared the ends of the DNA fragment for the ligation in the vector, which was cut with the same restriction enzymes. Thus, the DNA fragment matches specifically in only one possible orientation into the vector. Before the ligation, the DNA fragment was analyzed by gel electrophoresis and purified from the gel with a gel extraction kit (Thermo Fisher). Constructs cloned for this work were planned using Benchling software.

3.8.2.1. Overlap extension PCR

Overlap extension PCR is a combination of two consecutive PCRs with a unique primer design to, e.g., splice two DNA fragments [70]. In the first step, two DNA fragments are generated separately, whereby the reverse primer for the first fragment has an additional sequence at its 3'-end, which is complementary to the sequence of the 5'-end of the second fragment [70]. The forward primer of the second fragment has an additional sequence at its 5' end, which is complementary to the sequence of the 3' end of the first fragment [70]. In the second PCR, both amplified DNA fragments are pooled in one reaction together with the first fragment's forward primer and the second fragment's reverse primer. Thus, both strands of one DNA fragment have an overlapping sequence to the complementary strand of the other fragment and can hybridize after denaturation, and the fragment gets completed during elongation. The desired splice-fragment was validated by gel electrophoresis.

3.8.3. Ligation

The ligation of two DNA fragments is based on the T4-ligase enzyme, which can connect two adjacent nucleotides of one DNA strand through a phosphodiester bound (according to the manufacturer's product information). The requirement is that both DNA fragments were cut with the same two restriction enzymes and the restriction sites are in the same orientation on both DNA fragments (e.g., Mlu-1 at the 5' end and Not-1 at the 3' end). The ligation mix is incubated at RT for 1 hour followed by transformation (section 3.8.4.).

Reagent	**Volume ligation**	**Volume control**
T4-buffer	2,1 µl	2,1 µl
T4-ligase	0,4 µl	0,4 µl
Vector	1,5 µl	1,5 µl
Insert	6 µl	-
ddH_2O	11 µl	17 µl

3.8.4. Transformation and amplification of plasmid in bacteria

To amplify the desired plasmid, genetically modified bacteria (e.g., DH10, which is a non-pathogenic E.coli strain, or NEB-10β bacteria (bacteria strain which able to amplify large plasmids)) were used as small bioreactors which replicate a previously transformed plasmid multiple times [65]. The bacteria were stored at -80°C and thawed up slowly on ice. The bacteria suspension (50 µl) was split up into two parts. To one part, the plasmid was added (10 ng), and to the other half, 2 µl of RNAse free water was added as a control. After 15 min incubation on ice, both tubes were heat-shocked for 30 seconds in a 42°C warm water bath. Next, both probes were incubated on a Thermo shaker for one hour at 37°C after adding 700 µl SOC-medium, which is a growth medium for bacteria. Then 50 µl were taken from both probes and plated on an agar plate (without mixing both probes), which contained an antibiotic that matches the resistance gene in the plasmid, which should be amplified. Thus, only successfully transformed bacteria that incorporated the plasmid and transcribed the resistance gene in it can survive on this agar plate and can form colonies [26]. The plate was incubated overnight (12-24 h) at 37°C. The control side of the plate should be empty the next day, and the other half where the bacteria incorporated the plasmid should show small bacteria colonies, which were picked with a pipette tip and resuspended in 4 ml LB-medium (20 g/l and antibiotic 1:1000). This culture was also grown overnight at 37°C. The next day, the DNA of 1.5 ml of the bacteria suspension was extracted with the plasmid preparation kit of Thermo Fisher for mini cultures. The extracted DNA was analyzed by restriction digest and gel electrophoresis. If this showed the expected result, 250 µl of the mini culture were added to a midi culture, which has a volume of 250 ml. The DNA of this bacteria culture was extracted with the plasmid preparation kit of Qiagen for midi cultures or with the endotoxin-free plasmid preparation kit of Qiagen for midi cultures if the plasmid should be used for mouse zygote injections to reduce toxicity due to bacterial endotoxins for the mouse zygotes. The DNA was again analyzed by restriction digest and subsequent gel electrophoresis and sequencing.

3.8.5. Digest

The digest of a DNA fragment is based on the recognition of a specific sequence by its restriction enzyme [97]. Often the specific sequence is added to the primer sequence as an overhang so that the ends can be digested with the respective restriction enzyme and can be ligated with a vector that was linearized with the same restriction enzymes. The mix for a digest was incubated at 37°C (optimal working temperature of the enzymes according to the product information) for one hour.

Reagent	**Volume**
DNA	25 µl PCR-product or 2µg for analytic digest
10x Buffer NEB	3 µl
Restriction enzyme 1	0,5 µl
Restriction enzyme 2	0,5 µl
ddH_2O	ad 30 µl

3.8.6. Gel electrophoresis

DNA fragments can be separated by their length via gel electrophoresis [93]. The gel contains agarose, which polymerizes and forms pores when the gel cures [93]. The size of the pores is determined by the agarose concentration (1% for >500 bp and 1kb-marker; 2% for <500 bp and 50 bp-marker) in the gel [93]. The buffer which is used for the electrophoresis contains ethidium bromide, which intercalates with the DNA and fluoresces under UV light, thereby facilitating the visualization of DNA fragments in the gel after electrophoresis [93].

3.8.7. Sequencing

The sequencing of DNA fragments was done with the Sanger method [57]. This method is based on PCR with the difference that besides the normal nucleotides also di-deoxyribonucleoside triphosphates with a missing hydroxyl group are used, which are coupled to a fluorophore (in total 4 colors, for each nucleotide a different color) [57]. This missing hydroxyl group leads to termination during the elongation of a polynucleotide chain [57]. Due to the exponential increase of DNA fragments with the increasing number of cycles, there is at least one DNA fragment for each possible length [57]. These fragments are separated by capillary electrophoresis, and the fluorophore is stimulated by a laser beam [57]. Thus, this method uncovers at which position which nucleotide is present in the DNA sequence [57]. The analysis of the DNA fragments after the PCR was done by the Cologne Center of Genomics (CCG).

Reagent	**Volume**
Big Dye terminator v1.1/v3.1	0,25 µl
5x Big Dye Sequenzierungspuffer	2,25 µl
Sequenzierungsprimer (1pmol/µl)	0,25 µl
Plasmid	250 ng
+ ddH2O	ad 10 µl

Step	**Temperature**	**Duration**
(1) Denaturation	96°C	1 min
(2) Denaturation	96°C	10 s
(3) Annealing	55°C	5 s
(4) Elongation	60°C	4 min
Repetition of steps 2-4 39 times		
(5) Cooling	12°C	Forever

3.8.7.1. Enzymatic purification of PCR-products before sequencing

One reaction is pipetted as follows:

Reagent	**Volume**
SAP1	0.3 µl

EXO1	0.075 µl
ddH_2O	1.625 µl
PCR-product	8 µl

The mix is incubated at 37°C for 20 min for activation of the enzymes (EXO1/SAP1) and then at 72°C for 15 min for inactivation of the enzymes (according to the manufacturer's product information). 2 µl of this reaction are used for the Sanger sequencing reaction (2.8.7).

3.8.8. Materials for Cloning

Materials	**Manufacturer**
T4-Ligase + Buffer	Fermentas
Restriction enzymes	NEB
PCR Purification Kit	Thermo Fisher
Gel Extraction Kit	Thermo Fisher
SOC-medium	Invitrogen
DH-10 bacteria	Invitrogen
NEB-10β bacteria	NEB
LB-Medium	Roth
Ampicillin	Roth
Kanamycin	Roth
Ethidium bromide	Roth
Agarose	Sigma
TAE buffer: (25x stock solution) 121 g Trizma base, 28.5 ml acetic acid (100%), 18.6 g $Na_2EDTA\ 2H_2O$ → add ddH_2O to 1 l For 1x TAE buffer: 80 ml 25x TAE-buffer, 200 µl ethidium bromide (10 mg/ml), → add ddH_2O to 3.6 l	Nephrolab Roth Merck Sigma Applichem
1 kb DNA Marker	Thermofisher
50 bp DNA Marker	Thermofisher

3.8.9. Constructs cloned for this work

Name	Tag	Insert	Vector	Origin
AAV CAGGS eGFP-P2A-3XFLAG.hGlis2	eGFP-P2A-3xFLAG	*hGLIS2* (FL)	AAV CAGGS eGFP-P2A-3xFLAG	Nephrolab Cologne
AAV CAGGS eGFP-P2A-3xFLAG.hGlis2 (IVS5+1G>T)	eGFP-P2A-3xFLAG	*hGLIS2* (IVS5+1G>T)	AAV CAGGS eGFP-P2A-3xFLAG	Nephrolab Cologne
AAV CAGGS eGFP-P2A-3xFLAG.hGlis2 1-121	eGFP-P2A-3xFLAG	*hGLIS2* 1-121	AAV CAGGS eGFP-P2A-3xFLAG	Nephrolab Cologne
AAV CAGGS GFP-P2A-3xFLAG	GFP	P2A-3xFLAG	AAV CAGGS GFP	Nephrolab Cologne
His.mGlis2 (1-360) pET30b	His	*mGlis2* (1-360)	pET30b	Nephrolab Cologne
GST.mGlis2 (1-360) pGEX-4T3	GST	*mGlis2* (1-360)	pGEX-4T3	Nephrolab Cologne
GFP.mGlis2 FL WT pcDNA6	GFP	*mGlis2* FL WT	pcDNA6	Nephrolab Cologne
CRISPR: N-term tag mGlis2 Blasti.P2A.3xFLAG.spacer.emGFP.spacer pUC19	3xFLAG.spacer.emGFP.spacer		pUC19	Nephrolab Cologne

3.8.9.1. Used Constructs

Name	Tag	Insert	Vector	Origin
mGLIS2 Crispr No3 pSpCas9(BB)-2A-	GFP			Nephrolab Cologne

GFP				
hAAVS1 1L TALEN				Nephrolab Cologne
hAAVS1 1R TALEN				Nephrolab Cologne
AAV CAGGS EGFP	GFP			Nephrolab Cologne
F9.GFP pcDNA6	F9	GFP	pcDNA6	Nephrolab Cologne
V5.GFP pcDNA6	V5	GFP	pcDNA6	Nephrolab Cologne
GFP.NPHP9 WT pcDNA6	GFP	*NPHP9*	pcDNA6	Nephrolab Cologne
GFP.hNPHP7/GLIS2 WT FL pcDNA6	GFP	*hNPHP7* WT FL	pcDNA6	Nephrolab Cologne

3.9. Protein expression and purification

For the production of fusion protein, BL21 (RIPL+) bacteria were used, which are genetically modified in the way that they have a similar codon usage as mammalian cells like mouse cells [138]. This is crucial for the production of the correct peptide [138]. In this work, the produced peptide was later on used for injections in mice (Balb/C) to stimulate their immune system to produce antibodies against this peptide. First BL21 bacteria were transformed with the vector, which encodes for the fusion protein. One of the grown colonies was first cultured in a volume of 50 ml (LB-medium 20 g/l and kanamycin 1:1000 (pET30b vector encodes for a kanamycin-resistance)) overnight. 25 ml of this culture were added to a culture volume of 1 l. At an optical density of 0.6 (measured at 600 nm with a photometer), IPTG was added to a final concentration of 1 mM to further stimulate the peptide production in the BL21 bacteria [138]. The promotor which regulates the expression of the fusion protein can bind IPTG, which enhances the transcription of the gene encoding for the desired fusion protein [138]. The culture was then further incubated for 6 h at 30°C. Next, the culture was transferred to a Beckmann tube and spun down for 15 min with 11500 rpm at 4°C. The supernatant was then decanted, and the bacteria pellet was resuspended in 35 ml His-buffer. The resuspended bacteria could be stored like this at -20°C or further processed like described below.

The next step before the fusion protein can be specifically isolated by immunoprecipitation is the lysis of the bacteria. First, 350 µl of 100x DNAse-

/Lysozyme-mix (final concentrations 1 µg/ml DNAse and 200 µg/ml Lysozyme) were added to the bacteria resuspension and incubated for 15 min on ice. Right before sonication of the bacteria with a Branson sonicator, PMSF (phenylmethylsulfonyl fluoride) (100 mM) was added to a final concentration of 1 mM. PMSF is a protease inhibitor that prevents protein degradation by intracellular proteases (according to the product information). The resuspension was sonicated four times for 30 s with 35% power and a pulse length of 0.3 s (0.7 s pause). Next, the sonicated resuspension was transferred to a centrifugation tube and spun down for 45 min with approximately 50000 g at 4°C. After that, the supernatant was filtered with a 0.45 µm filter and stored at 4°C. 1 ml of this protein solution was taken, and the fusion protein was detected by immunoprecipitation with nickel-beads (30 µl) (for His-tagged fusion protein) and gel electrophoresis with subsequent Coomassie staining of the gel. This is a test to prove if the peptide production worked and if it is worthy to isolate fusion protein from the whole bacteria lysate. If the fusion protein with the expected size is detectable, the fusion protein is isolated from the whole bacteria lysate. First, the supernatant was spun down for 5 min with 4000 rpm at 4°C. If a small pellet appeared again, the supernatant above was isolated again. Next, the supernatant was incubated with 100 µl nickel-beads (for His-tagged fusion protein) overnight at 4°C. The next day the beads were spun down for 5 min with 4000 rpm at 4°C. The supernatant, which should not contain fusion protein anymore, was saved and later on loaded together with a small part of the eluate, which should contain fusion protein to show that the nickel beads precipitated all available fusion protein of the bacteria lysate. The beads pellet was then resuspended in 10 ml His-buffer and gradually applied on a protein purification column (1 ml) which consists of a filter that prevents the beads from running through the column. The column was washed three times with 10 ml His-buffer. Finally, the fusion protein was eluted from the column by an elution buffer which consists of His-buffer plus 300 mM imidazole, which replaces the fusion protein as a binding partner of the nickel-beads [18,154]. The volume of 800 µl elution buffer was applied in 100 µl steps (8x 100 µl) to exclude certain eluates that do not contain fusion protein which was proven later on by gel electrophoresis and Coomassie staining. Finally, the column purified fusion protein was further purified by dialysis in a dialysis chamber surrounded by 1x PBS (4°C). This step was performed to exclude contaminants and to minimize toxic side effects on mice through the injection of the fusion protein in the frame of generation of a monoclonal anti-GLIS2 antibody.

3.9.1. Material for protein expression and purification

Material	Manufacturer
Ni-NTA Agarose beads	Invitrogen (#R901-01)
Anti-GST-beads	Amersham Biosciences (17-5132-01)
IPTG	AppliChem
DNase/Lysozyme mix	Appli Chem
Protein purification column (1ml)	Quiagen
Dialysis chamber	Thermo Fisher
BL21 (+RIPL)	Thermo Fisher
Photometer	

3.9.2. Coomassie staining

The Coomassie staining is a method to stain denatured protein in a polyacrylamide gel after gel electrophoresis [136]. First, the gel cassette was removed, and the collecting gel (upper part of the gel) was severed. After that, the polyacrylamide gel was incubated for 30 min in fixation solution on a shaker. After three washing steps with desalted water, the gel was stained overnight with Coomassie staining solution on a shaker. The next day the gel was freed of abundant staining solution by incubation in desalted water for 6 hours (the water was changed every 2 hours). Then the staining pattern of the gel could be judged and was digitalized by a scanner.

3.9.2.1. Materials for Coomassie staining

Material	Manufacturer
Fixation solution: 250 ml Isopropanol, 100 ml acetic acid, → add ddH_2O to 1 l	Nephrolab Sigma Roth
Colloidal Coomassie staining solution: 100 g ammonium sulfate, 1 g Coomassie brilliant blue G-250, 30 ml ortho-phosphoric acid → add ddH_2O to 1 l	Nephrolab Roth Bio-Rad
Gel scanner (Odyssey CLx)	LI-COR

3.10. Generation of hybridoma cells

Köhler and Milstein first published a method for the production of monoclonal antibodies [87]. The technique is based on the fusion of multiple myeloma cells (a tumor of plasma cells) with murine B-cells of mice which were immunized with a specific antigen (80 µg per injection) two times with an interval of one week [64]. Those cells are called hybridoma cells [64]. The cells are fused using polyethylene glycol (PEG), which enables the fusion of cell membranes [64]. The myeloma cells are selected beforehand regarding their deficiency of antibody production and the enzyme hypoxanthine-guanine phosphoribosyltransferase (HGPRT) [95]. The absence of this enzyme makes the myeloma cells sensitive for medium containing hypoxanthine-aminopterin-thymidine (HAT) [95]. The consequence is that unfused murine B-cells die after a few days in culture because they are not immortalized, and unfused myeloma cells die because of their sensitivity to HAT medium [95]. Thus, only hybridoma cells can survive under this condition [95]. The hybridoma cells are singularized by single-cell dilution and analyzed regarding the specificity of their produced monoclonal antibody by ELISA, WB, and IP. As part of this work, the immunization of two different mice was done by Gisela Slaats, Ph.D., and the generation of hybridoma cells and the culturing of those was done by Prof. Dr. Bernhard Schermer.

3.11. ELISA

ELISA is a method to detect an antibody with specificity for a particular antigen [10]. The principle is very similar to western blot, which was described before. Special 96-wells (Nunc Maxisorb stripes in frame) were used for this ELISA test. The bottom of these 96-wells can bind protein [10]. First, the ELISA plate was coated with a defined antigen (60 ng protein in 100 µl PBS per well). Therefore, the plate was incubated at 4°C overnight. The next day the plate was washed once with PBST and blocked for one hour with PBS + 1% BSA (100 µl per well) at room temperature. After that, the plate was washed three times with PBST to eliminate excess blocking solution. Next, the plate was incubated for one hour at 37°C with different probes, which should be tested respectively their content of antibodies which are targeting the antigen the ELISA plate was coated with. As part of this work, culture media of different hybridoma clones, which contained antibodies secreted by the hybridoma cells, were tested. The ELISA plate was washed three times again with PBST. Thereafter, the plate was incubated for one hour at room temperature with an anti-IgG antibody coupled to horseradish peroxidase (1:5000 in PBST; 100 µl per well). Afterward, the plate was washed three times again with PBST. Finally, a developer solution was added to the wells of the plate to visualize in which well the secondary antibody was still present because of sufficient binding between antigen and the first antibody. If the first antibody is still bound to its antigen, the secondary antibody has bound to the Fc domain of the first antibody, and the horseradish peroxidase coupled to the secondary antibody oxidizes TMB, which is contained in the developer solution [10]. Through this oxidation, TMB turns blue [10]. The reaction was stopped by addition of 2 M HCl when the positive control showed a solid blue color. HCl turns the color into yellow. In the end, the intensity of the color reaction was quantified by absorption measurement at 450 nm using a multimode plate reader.

3.11.1. Materials for ELISA

Material	**Manufacturer**
BSA	
PBST (PBS + 0,05% Tween)	
Anti-mouse IgG (H+L) (see above) (1:5000 in PBST)	Jackson ImmunoResearch
Developer solution: 50 mM sodium acetate (pH 5), TMB (0,01 mg/ml), 0,013% H_2O_2 → in ddH2O	 Sigma Roth
HCl 2 M	Merck
Maxisorb stripes in frame	Nunc
Multimode plate reader EnSpire	Perkin Elmer

3.12. Generation of a monoclonal stable cell line using CRISPR/Cas9

CRISPR/Cas9 is a genome editing system that is based on mechanisms of the adaptive immune response of bacteria to prevent the integration of virus DNA [61]. The system consists of the Cas9 enzyme, which can bind RNA and cut double-stranded DNA, and a guide RNA which is derived from the transcription of integrated virus DNA or a synthetized guide RNA in a biotechnical context [124]. Cas9 binds the guide RNA, which hybridizes due to its sequence with a specific genomic region, thus recruiting the Cas9 enzyme to this region and bringing it in close proximity to the DNA double-strand, which then can be cut by Cas9 [124]. As a result, this system makes it possible to target nearly every genomic region specifically by only designing and synthesizing the respective guide RNA [124]. As part of this work, this system was used to create a monoclonal stable knock-in line where the sequence for a protein tag was knocked in right before the ATG of the gene of interest resulting in an endogenous fusion protein.

Therefore, mouse IMCD3 cells were transfected with two plasmids using lipofectamine 2000 (0.25 µg of both plasmids for one 24-well together with 50 µl Optimem and 1.5 µl lipofectamine). One plasmid encoded for the guide RNA and Cas9 coupled to GFP via a 2A-peptide. The 2A-peptide is disrupted during translation resulting in two separate proteins (Cas9 and GFP). The other plasmid encoded for the tag sequence, which should be integrated right before (5') the ATG and is flanked by a 5' and a 3' homology arm, which mediate the recruitment of the repair template to this specific genomic region. One week after transfection, the cells were FAC sorted like described below.

3.12.1. Fluorescence-activated cell sorting

Eukaryotic cells which express a fluorescent protein (mostly genetically modified cells) can be separated from non-fluorescent cells by fluorescence-activated cell sorting (FACS) [1]. The technology is based on flow cytometry and a set of lasers with different wavelength spectra, which can stimulate fluorescent proteins to emit light of a certain wavelength spectrum [1]. As part of this work, this technique was used to create a transgenic monoclonal cell line using CRISPR/Cas9. The plasmid that encoded for Cas9 contained a GFP-reporter which served as a distinctive feature between sufficiently transfected and non-transfected cells. Two days after transfection, the cells were detached with trypsin and resuspended in medium. Next, they were spun down with 500 g for 3 min at room temperature. The supernatant was aspirated, and the pellet was resuspended in FACS-buffer (PBS with 2% FBS). The cells were transported like this to the BD FACSAria IIIu Svea (100 µm nozzle), which is in this case located in the MPI for Aging (Cologne). Finally, the fluorescent cells were separated from the non-fluorescent cells and sorted into 96-wells (one fluorescent cell per well; cultured with penicillin and streptomycin to prevent contamination by bacteria or fungi) to create monoclonal cell clones, which were further analyzed by integration PCR, WB, IP, and IF.

3.12.2. Lysis of monoclonal CRISPR cells for subsequent integration-PCR

The cells were grown in 96-well plates. After splitting once 1:1 in 24-well plates, the cells were lysed for subsequent integration-PCR by removing the medium and adding 30 µl lysis buffer. The cells were incubated for 5 min on a shaker at room temperature, and the extracts of every well were transferred to PCR tubes. Finally, the extracts were incubated for one hour at 56°C and 10 min at 95°C.

3.12.2.1. Materials for lysis of monoclonal CRISPR cells

Material	**Manufacurer**
Lysis buffer: 10 mM Tris-HCl pH 8.3, 0.45% Tween, 0.45% Triton-X,	Nephrolab

100 µg/ml proteinase K, 50 mM KCl, 2.5 mM $MgCl_2$	Fluka Roth Merck

3.13. Generation of polyclonal stable cell lines using TALEN

The Transcription Activator-like effector nucleases (TALEN) are fusion proteins that consist of a TAL-effector domain that mediates DNA binding and a nuclease domain that facilitates cutting of DNA [76]. Depending on their TAL-effector domain, the TALENs function as sequence-specific restriction enzymes [76]. Thus, eukaryotic cells can be transfected with the plasmids encoding for both TALEN enzymes (both enzymes cut in the same genetic locus (e.g., AAV locus (reported to be a save harbor locus in the genome of human cells)) in close proximity to each other; 0.5 µg of each plasmid was transfected) and a repair template (1 µg of the repair template was transfected) which is integrated into the endogenous DNA via the homology-directed repair pathway [76]. The plasmid with the DNA sequence, which should be integrated into the cell genome, is flanked by two homology arms (at the 5' and 3' of the sequence) which mediate the integration of this sequence [76]. In most cases, the DNA sequence which is integrated encodes for a fusion protein that consists of a tag peptide and a protein of interest. The result is a pool of untagged endogenous protein and a pool of tagged protein that is transcribed from the integrated DNA sequence, which consists of the coding sequence for the protein of interest and the tag sequence. Thus, the protein of interest can be investigated in a more stable and physiological status as under overexpression conditions. Furthermore, a puromycin resistance gene was integrated together with the sequence of the fusion protein. Thus, the cells could be selected for positive integration of the repair template through the addition of puromycin (final concentration 4 µg/ml) to the medium. The selection was started 24 h after transfection. The cell lines were further validated by integration-PCR, IF and used for mass spectrometry analysis.

For lysis of TALEN cells for subsequent integration PCR, one tenth of a 6-well was resuspended in 20 µl quantilyse buffer after washing the cell pellet once with PBS. The resuspended pellet was then incubated for 30 min at 50°C and then further incubated for 10 min at 90°C. Finally, the sample was further diluted (1:1000). 1 µl of this dilution was added to the PCR as a template.

3.13.1. Materials for generation of polyclonal stable cell lines using TALEN

Material	Manufacturer
Quantilyse buffer: 10 mM Tris, 5 µM SDS, 10 µg/µl proteinase K	Nephrolab

4. Results

4.1. Generation and analysis of homemade hybridoma clones regarding their anti-GLIS2 antibody production

Before starting the generation of a homemade anti-GLIS2 antibody by hybridoma culture, we tested an existing commercial polyclonal anti-GLIS2 antibody (Atlas Antibodies (HPA056976)) regarding its suitability for applications like WB, IP, and IF staining. It turned out that the tested antibody was only able to detect overexpressed but not endogenous GLIS2 in western blot sufficiently. It was not suitable IP and IF staining.

As the commercial anti-hGLIS2 antibody turned out to be not suitable for the desired downstream applications, we tried to generate a homemade monoclonal anti-GLIS2 antibody. Therefore, we cloned the first 120 base pairs (N-terminus) of the coding sequence of the mouse *Glis2* gene into a pET30b vector. This plasmid results in an N-terminally His-tagged fusion protein after transformation and consecutive protein production in BL21 (+RIPL) bacteria. The first 360 base pairs of the coding sequence of *Glis2* were chosen because this part excludes the zinc finger domains of GLIS2, which are common conserved domains among DNA-binding proteins. If the sequence for the zinc finger domains were included in the cloned fragment, the risk of generation of cross-reactive antibodies targeting zinc finger domains would be high. The His-tag was chosen because of its low immunogenicity to avoid the generation of antibodies targeting the protein tag [154]. Figure 2 A shows the results of purification of the His.mGLIS2 (aa. 1-120) protein after immunoprecipitation and column purification of BL21 (+RIPL) bacteria lysates with consecutive SDS-page gel electrophoresis and coomassie staining. The fusion protein has a size of approximately 19 kDa. The fusion protein (prepared with an adjuvans) was injected into the hind limb of two different mice (Balb/C). After several injections, the serum of both mice was tested for polyclonal antibodies against GLIS2 via western blot. Figure 2 B shows that the polyclonal antibodies in the serum of both mice can specifically detect GFP.mGLIS2 expressed in HEK293T cells. GFP.hGLIS2 is not detected, GFP.NPHP9 served as a negative control. As described in the methods, the B-lymphocytes of the popliteal lymph node of the hind limb, where the fusion protein was injected, are fused to myeloma cells using PEG. After single-cell dilution and selection of hybridoma cells in cell culture, the clones each deriving from a single hybridoma cell were analyzed. In total, 473 clones were tested in ELISA, 193 clones were tested in western blot, and 27 clones were tested for immunoprecipitation. The ELISA test (Table 1) was used as the first screening method to examine the ability of the monoclonal antibody to bind native

GLIS2 protein. The wells were coated with GST.mGLIS2 (aa. 1-120) to avoid false-positive results that might be caused by anti-His-tag antibodies. The three most promising clones (highest absorption value) were clones D1, D40, and E27 on this plate. Next, the ability to bind denatured GFP.mGLIS2 was tested via western blot using a special multi-blot device (for incubation of distinct areas of the membrane with supernatants of different hybridoma clones). Clones D1, D40, and E27 show either no detection of any protein (D1) or very unspecific detection of many different proteins (D40 or E27) and all of them were not able to detect specifically GFP.mGLIS2 (Figure 2 C). Immunoprecipitation examines the capability of an antibody to bind a specific native protein. This ability is also essential for downstream applications like ChIP-seq or interactome analysis using mass spectrometry, as these techniques require a sufficient immunoprecipitation of a specific protein. Hence, the monoclonal antibodies contained in the supernatants of the respective hybridoma clones were coupled to protein G-coated beads to test their ability to precipitate native GFP.mGLIS2. In Figure 2 D, there is an unspecific band around 100 kDa visible, which is slightly higher than the band which is specific for GFP.mGLIS2. This one is visible in the lysate and the immunoprecipitation of GFP.mGLIS2 with an anti-GFP antibody, where GFP.mGLIS2 is strongly enriched compared to the lysate. All tested monoclonal antibodies of the different clones only show this unspecific band, which is more intense for clone D1. In conclusion, none of the 473 clones matched the detection requirements of native or denatured mGLIS2 in WB or IP.

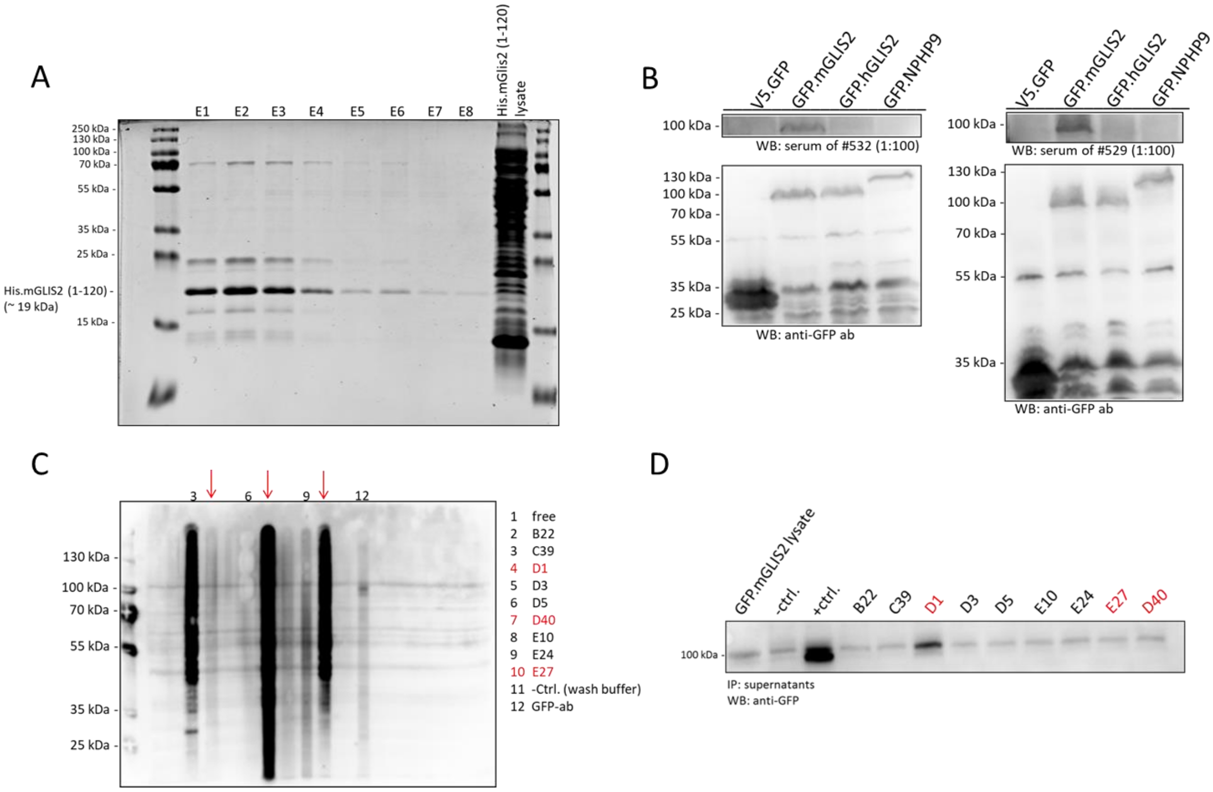

Fig. 2: Generic workflow for analysis of hybridoma clone supernatants

A Eluates of N-terminally His-tagged truncated mGLIS2 (aa 1-120) after immunoprecipitation and column purification analyzed by SDS-page gel electrophoresis and subsequent Coomassie staining. **B** Western blot of lysates of HEK293T cells overexpressing GFP.mGLIS2, GFP.hGLIS2, GFP.NPHP9 and V5.GFP. Staining with serum of mice #529 and #532 and re-staining of the membrane was performed with an anti-GFP antibody. **C** Western blot of lysate of HEK293T cells overexpressing GFP.mGLIS2 stained with supernatants of hybridoma clones, 3 minutes exposure time **D** IP of GFP.mGLIS2 from lysates of HEK293T cells overexpressing GFP.mGLIS2 by supernatants from clones tested in the western blot. In the negative control, an anti-V5 antibody and in the positive control, an anti-GFP antibody was used for the pull-down.

C24 0,163	**C32 0,102**	**C40 0,247**	**D8 0,119**	**D16 0,147**	**D24 0,124**	**D32 0,117**	**D40 1,769**	**E8 0,461**	**E16 0,134**	**E24 0,416**	**neg. ctrl. PBST 0,124**
C23 0,145	**C31 0,122**	**C39 0,591**	**D7 0,156**	**D15 0,209**	**D23 0,188**	**D31 0,119**	**D39 0,173**	**E7 0,190**	**E15 0,134**	**E23 0,129**	**Serum of #529 (1:1000) 1,842**
C22 0,162	**C30 0,123**	**C38 0,132**	**D6 0,116**	**D14 0,263**	**D22 0,118**	**D30 0,120**	**D38 0,118**	**E6 0,122**	**E14 0,373**	**E22 0,118**	**E30 0,130**
C21 0,133	**C29 0,125**	**C37 0,329**	**D5 0,326**	**D13 0,195**	**D21 0,131**	**D29 0,201**	**D37 0,116**	**E5 0,258**	**E13 0,133**	**E21 0,124**	**E29 0,133**
C20 0,140	**C28 0,134**	**C36 0,130**	**D4 0,124**	**D12 0,116**	**D20 0,119**	**D28 0,138**	**D36 0,165**	**E4 0,128**	**E12 0,168**	**E20 0,124**	**E28 0,141**
C19 0,121	**C27 0,119**	**C35 0,129**	**D3 0,829**	**D11 0,138**	**D19 0,249**	**D27 0,117**	**D35 0,123**	**E3 0,589**	**E11 0,112**	**E19 0,119**	**E27 1,647**
C18 0,122	**C26 0,157**	**C34 0,130**	**D2 0,123**	**D10 0,121**	**D18 0,112**	**D26 0,121**	**D34 0,146**	**E2 0,151**	**E10 0,294**	**E18 0,138**	**E26 0,165**
C17 0,117	**C25 0,134**	**C33 0,165**	**D1 1,397**	**D9 0,134**	**D17 0,145**	**D25 0,153**	**D33 0,150**	**E1 0,133**	**E9 0,138**	**E17 0,163**	**E25 0,314**

Table 1: Evaluation of hybridoma supernatants by ELISA

Readout of an absorption measurement at 450nm. The GST.mGLIS2 (aa 1-120) coated plate was incubated with the supernatants of the different hybridoma clones, each in a separate well. Clones with an absorption value above 1 are depicted in red. 94 clones were tested on this plate together with the serum of mouse #529 as positive control and PBST as a negative control.

4.2. 3xFLAG.emGFP.GLIS2 fusion protein is expressed at very low levels

In parallel to the attempt to generate a homemade anti-mGLIS2 antibody, the generation of an IMCD3 GFP-FLAG-knock-in GLIS2 cell line using CRISPR/Cas9 was an alternative strategy to circumvent the problem of GLIS2 isolation from cell lines or kidney tissue for further biochemical analysis. For precise genome editing, we used the repair template (HA-Blasti.P2A.3xFLAG.spacer.emGFP.spacer-HA pUC19) (Figure 3 A). Mouse inner medullary collecting duct cells were chosen for the generation of this cell line as they are ciliated and represent a renal cell type which is thought to play a crucial role in the pathophysiologic mechanisms occurring during the development of the renal phenotype of NPH [59]. The blasticidin resistance gene was included in the insert to have the opportunity of antibiotic-based selection for cells that are positive for integration of the insert (Figure 3 A). The 3xFLAG-tag is encoded 5' to the sequence of emGFP resulting in a 3xFLAG-tag at the N-terminus of the 3xFLAG.emGFP.GLIS2 fusion protein to maintain the accessibility of the 3xFLAG-tag for anti-FLAG antibodies. The cells were FAC-sorted based on GFP expression encoded by the transfected plasmid for Cas9 and the sgRNA targeting the ATG of the *Glis2* gene (mGLIS2 Crispr No3 pSpCas9(BB)-2A-GFP). 192 growing cell clones were obtained and screened for positive integration by integration PCR after extraction of genomic DNA of each cell clone (Figure 3 B). 14 of those showed a band of the expected size in the integration PCR and were further analyzed by Sanger sequencing of the region between the 3' end of the insert and the ATG of the first coding exon (counted as exon 1, two exons are 5' of this one but do not contribute to the coding sequence of the *Glis2* gene). Only one clone (#46) of the sequenced ones turned out to have an error-free transition between the integrated sequence and the endogenous *Glis2* coding sequence (not shown). Clone #46 was then further tested for expression of 3xFLAG.emGFP.GLIS2. Fluorescence microscopy (Zeiss LSM710) of cells from clone #46 did not show detectable GFP-mediated fluorescence, and those were also negative for anti-FLAG immunofluorescence staining (not shown). The detection of an anti-FLAG immunoprecipitation of 3xFLAG.emGFP.GLIS2 via western blot was also unsuccessful (not shown). Finally, targeted mass spectrometry, which is one of the most sensitive methods for detection of a specific protein from a cell lysate, was used to detect the fusion protein from an anti-FLAG immunoprecipitation of 3xFLAG.emGFP.GLIS2. Twenty 10 cm dishes per cell line were used (Figure 3 C). Peptides specific for the fusion protein (peptides from the region between the insert and endogenous *Glis2* sequence containing amino acids of the spacer and the first amino acids from the GLIS2 protein) were detected. However, the result also reflects the fact that the amount of expressed 3xFLAG.emGFP.GLIS2 is very low. One reason for this is the heterozygosity which was proven by the amplification of a wild-type band and a transgenic band (forward primer binds 5’ of the insert and reverse primer binds 3’ of the insert) via PCR. However, GLIS2 might, in general, be a very low abundant protein. The extremely small amount of tagged GLIS2 makes this cell line unsuitable for desired downstream applications like mass spectrometry-based interactome analysis, ChIP-seq, or nuclear laser ablation experiments using multiphoton microscopy as all of those methods require higher expression levels.

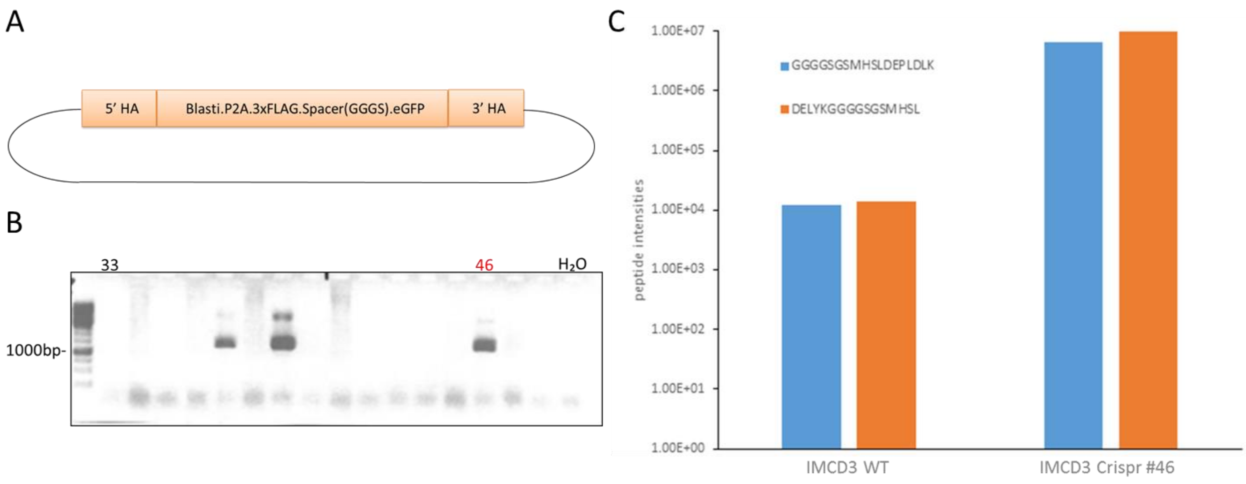

Fig. 3: Validation of IMCD3 3xFLAG-emGFP-KI GLIS2 CRISPR line

A The design of the targeting vector. The 'insert' was embedded in a pUC19 vector surrounded by a 5' and a 3' homology arm. **B** Cell clones were tested by PCR to validate integration. A forward primer binding to the sequence of emGFP (GFP646/664fsp) and a reverse primer binding to the sequence of *Glis2* (mGlis2 Surveyor NRP2) (binds in intron 1, which is not part of the 3' homology arm of the repair template) was used to generate a fragment of 1222bp size. **C** Mass spectrometry analysis was performed to detect the fusion protein after FLAG-immunoprecipitation of clone #46. Trypsin (blue) and Asp-N (orange) were used to digest the proteins in the sample, and fusion protein-specific peptides were searched. Peptide intensities under 10^5 are not significant and are interpreted as background noise level.

4.3. Single copy integration of GFP.P2A.3xFLAG.GLIS2 and GLIS2 mutant variants

As the generated monoclonal IMCD3 3xFLAG.emGFP-knock-in GLIS2 CRISPR cell line turned out to be not suitable for any of the desired downstream applications we used a TALEN-based genome editing system to create a polyclonal HEK293T-based cell line expressing GFP.P2A.3xFLAG.GLIS2 by single copy integration in the *AAVS1* locus. The P2A-peptide between GFP and 3xFLAG facilitates cleavage during translation of the fusion protein via ribosome skipping [96]. Thus, a 3xFLAG-tagged GLIS2 protein and GFP are expressed in equimolar amounts. GFP mainly serves as a reporter protein during the validation of the cell lines. In addition, we generated one cell line mimicking a published point mutation (IVS5+1G>T) and a second one missing all zinc finger motifs (only the first 121 N-terminal amino acids) [7]. Both variants result in a truncated GLIS2 protein. Those cell lines were called HEK293T GFP.P2A.3xFLAG.GLIS2 (IVS5+1G>T) and HEK293T GFP.P2A.3xFLAG.GLIS2 1-121 (Figure 4 A). The patient mutation IVS5+1G>T is a point mutation at the beginning of the sequence of intron five of the *GLIS2* gene, which destroys the donor splice site. This can result in many possible GLIS2 variants depending on the way the resulting mutated pre-mRNA is further processed. We postulated a processing variant where the translation of the *GLIS2* mRNA is terminated by a stop codon occurring in the middle of intron 5. This scenario was modeled by the cell line, expressing 3xFLAG.GLIS2 (IVS5+1G>T). Therefore, the sequence of intron 5 until the first stop codon (251 bp) was amplified from human DNA and was fused to the coding sequence of the first five exons by overlap extension PCR and cloned into the AAV CAGGS GFP-P2A-3xFLAG vector. After transfection of the repair template and both TALEN arm plasmids, the resulting cell lines were first tested for integration events in the AAVS1 locus by integration PCR (not shown). Next, the cell lines were evaluated for GFP-mediated green fluorescence and the presence of FLAG-tagged fusion protein by fluorescence microscopy (Figure 4 B). A HEK293T GFP.P2A.3xFLAG cell line served as a control. The anti-FLAG immunofluorescence staining shows the subcellular localization of the different GLIS2 variants. In summary, the full-length variant shows a nuclear staining pattern, whereas the GLIS2 1-121 truncation shows a cytosolic accentuated staining pattern that omits the nucleus. This is consistent with the current understanding of GLIS2 structural biology that the third zinc finger domain is required for translocation to the nuclear compartment [145]. The staining pattern of the GLIS2 IVS5+1G>T truncation is not specific for a subcellular compartment and is more distributed all over the cell, but in some cases, it also shows a nuclear-accentuated staining pattern.

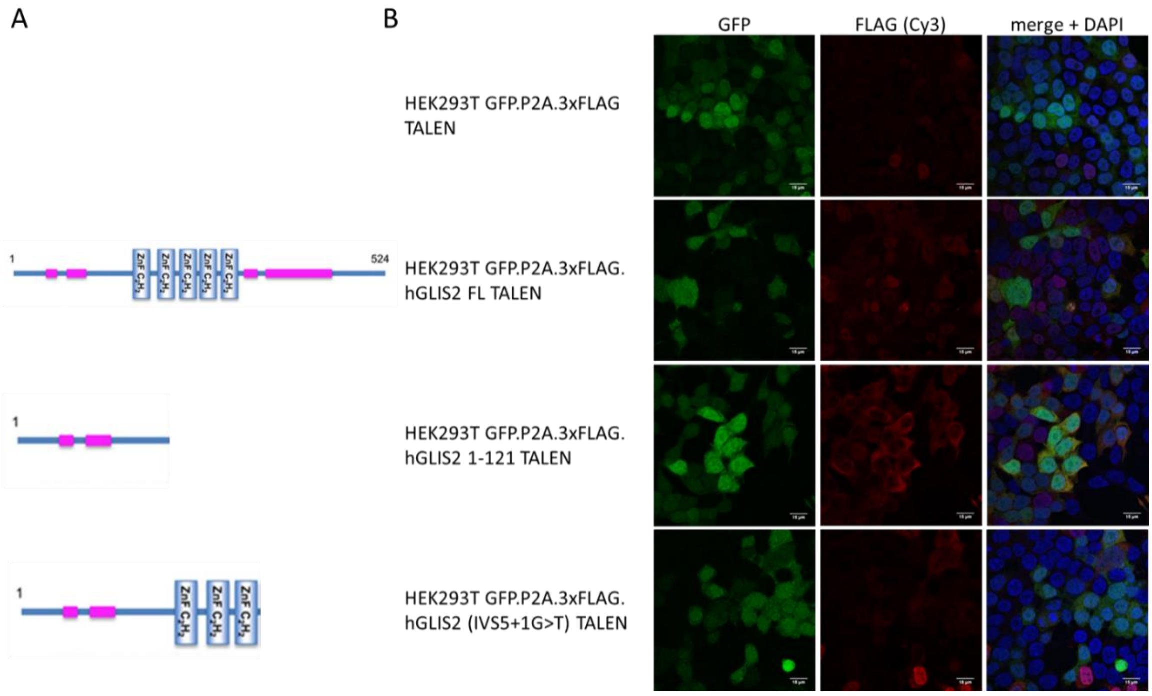

Fig. 4: Validation of polyclonal HEK293T GLIS2 TALEN cell lines via immunofluorescence staining
A Visualization of domains that are abrogated in the different truncations. The shortest truncation (1-121) lacks all zinc-finger domains. The IVS5+1G>T truncation still has three of the five zinc finger domains. The scheme of the part of GLIS2 which is expressed in the respective TALEN cell line is in the same row as the IF pictures of the respective cell line (scheme from Ramachandran, H., et al., *The C175R mutation alters nuclear localization and transcriptional activity of the nephronophthisis NPHP7 gene product.* Eur J Hum Genet, 2016. **24**(5): p. 774-8. [123]). **B** The TALEN cell lines were stained with an anti-FLAG antibody and a secondary antibody coupled to a Cy3-fluorophore. The slides were imaged with Zeiss LSM710 confocal microscope. Scale bar = 5 µm

4.4. Interactome analysis of GLIS2

As the goal of this work was to further characterize functions of GLIS2, mass spectrometry-based analysis of FLAG-immunoprecipitations of all four generated cell lines was performed. The truncated TALEN cell lines were generated to find out which protein interactions are lost if only the first five exons are correctly translated (HEK293T GFP.P2A.3xFLAG.GLIS2 (IVS5+1G>T)) or when all five zinc finger domains are absent (HEK293T GFP.P2A.3xFLAG.GLIS2 1-121) compared to the protein interactions of the full-length GLIS2 protein. The FLAG-immunoprecipitations of four replicates were derived from four different passages (p. +2, +4, +6, +8). It is important to note that mass spectrometry-based analysis of protein interactors not only reveals proteins that are in direct physical interaction with GLIS2 but also proteins that are part of the same protein complex as GLIS2. After FLAG-immunoprecipitation, digestion of the proteins, and mass spectrometry measurement, the raw mass spectrometry data was quantified and normalized with MaxQuant software and was further analyzed with Perseus version 1.5.5.3 [30,31,143]. Fast Pearson correlation between the samples was performed as quality control. The clustering of the samples based on similarity regarding the peptide composition of the sample was visualized in a heat map (Figure 5 A). In each case, samples of the GLIS2 FL cell line, the GLIS2 IVS5+1G>T line, and the control line are clustering nicely together, which shows the similarity of the samples of one cell line as expected. Only samples of the GLIS2 1-121 cell line are not clustering in a separate group and are distributed over the three other groups. This observation reflects the fact that the set of proteins which is detected in samples of the GLIS2 1-121 line shares a partial similarity with the other two GLIS2 TALEN lines. The small number of significant interactors of the GLIS2 1-121 line also explains the partial similarity to the control line. The interactome analysis revealed 477 significant interactors for the cell line, expressing 3xFLAG.GLIS2 FL, 15 significant interactors for the cell line, expressing 3xFLAG.GLIS2 1-121, and 450 significant interactors for the cell line, expressing 3xFLAG.GLIS2 (IVS5+1G>T). The overlap regarding significant protein interactors of 3xFLAG.GLIS2 FL and 3xFLAG.GLIS2 (IVS5+1G>T) adds up to 412. These two lines show to have a common subset of protein interactors which are localizing in the nuclear compartment like Poly (ADP-ribose) polymerase 1 (PARP1), DNA repair protein RAD50 (RAD50), DNA-dependent protein kinase catalytic subunit (PRKDC), and DNA polymerase delta (POLD1) (interacts with the catalytic subunit of POLD1), X-ray repair protein 5 (XRCC5, Ku80), XRCC6 (Ku70) and DNA-ligase 3 (LIG3) [25,114]. Table 3 lists central DDR proteins found in the interactome of 3xFLAG.GLIS2 FL. This finding is also consistent with our immunofluorescence staining where 3xFLAG.GLIS2 FL and 3xFLAG.GLIS2 (IVS5+1G>T) showed a nuclear-accentuated staining pattern and suggested that this interaction occurs in the nuclear compartment. Comparison with a published nuclear proteome shows that about one quarter of the significant interactors of 3x.FLAG.GLIS2 FL is localizing to the nuclear compartment (Figure 6 B) [41]. However, proteins that are reported to be part of the ciliary proteome generated by proximity labeling (APEX) are also found in this interactome (Venn diagram in Figure 6 A and details in section 5.4.) [88,108]. Among the GLIS2 interactors, there are 64 proteins (of 301 proteins in total) which were also found to be part of the ciliary proteome in the study of Kohli *et al.* (2017), and 62 proteins (of 370 proteins in total) which were part of the ciliary proteome published by Mick *et al.* (2015) [88,108]. Those two groups of proteins share an overlap of 18 proteins which are found in both ciliary proteomes and the GLIS2 interactome. These findings provide some evidence for the ciliary role of GLIS2. Hence, GLIS2 seems to play a dual role in nuclear and ciliary processes. The top 30 interactors (depicted in red in the half volcano plots), which were defined by the 30 highest values for the multiplication of the log_2LFQ-value and the respective log_{10} of the negative p-value are listed (for 3xFLAG.GLIS2 FL and 3xFLAG.GLIS2 (IVS5+1G>T)) in table 2 (A-C). Gene ontology term enrichment analysis regarding biological processes was also performed and revealed roles of GLIS2 in the regulation of G-protein signaling and actin dynamics (section 7.3.) particularly. Of course, GO-term enrichment analysis has limited validity in the context of interactome analysis and should be therefore judged with caution.

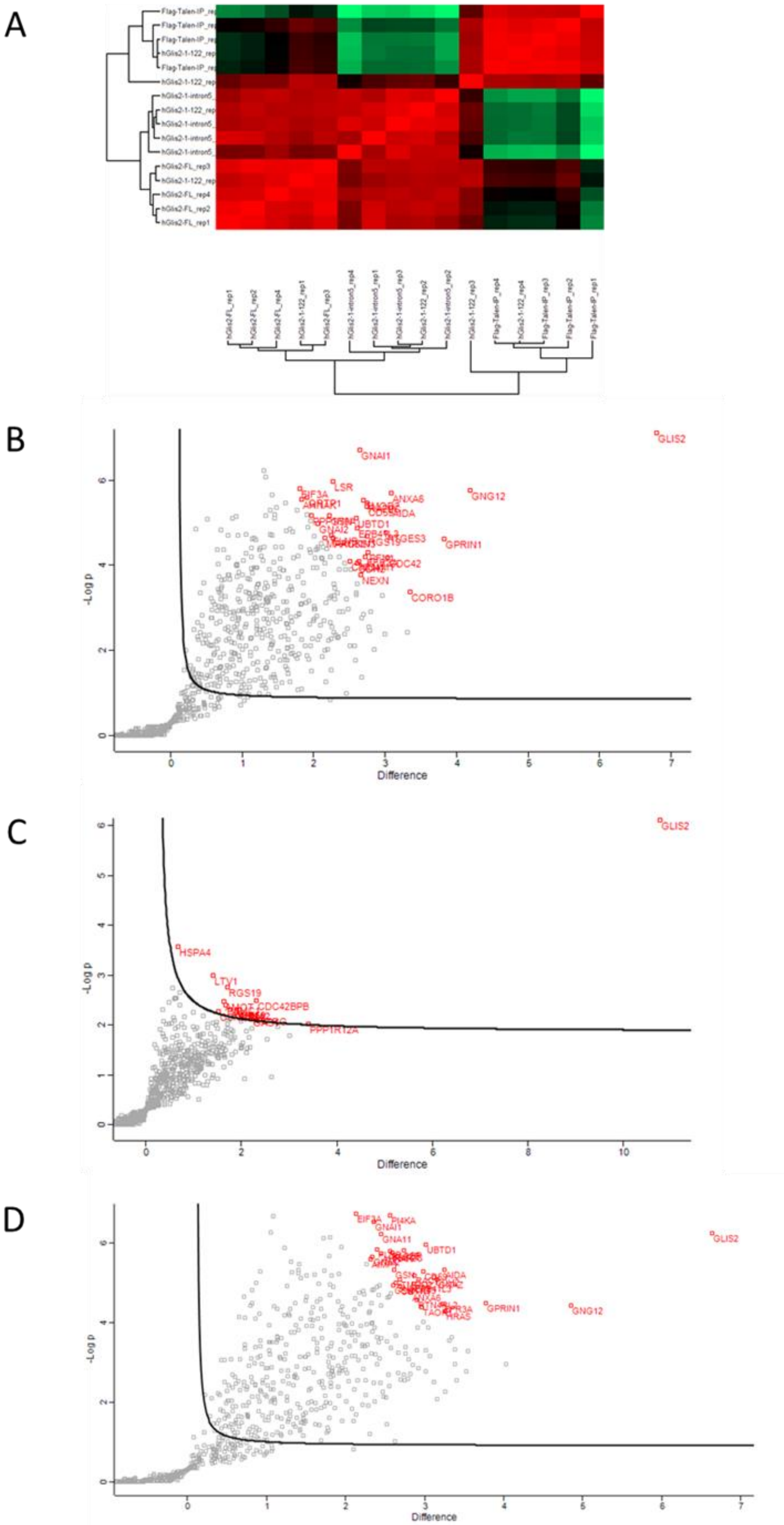
A
B
C
D
-Log p
Difference
GLIS2
GNAI1
LSR
EIF3A
ANXA6
GNG12
UBTD1
GPRIN1
CDC42
NEXN
CORO1B
HSPA4
LTV1
RGS19
CDC42BPB
PPP1R12A
PI4KA
GNA11
HRAS

Fig. 5: FLAG-immunoprecipitation of polyclonal HEK293T GLIS2 TALEN cell lines with subsequent mass spectrometry-based interactome analysis

A Heat map visualizes the extent of similarity regarding the set of detected proteins of one sample compared to the other samples (high similarity=red, low similarity=green) based on fast Pearson correlation. Hierarchical clustering of the samples is based on Euclidean distance. **B C D** The volcano plots show logarithmized (log_2) fold change of LFQ values measured in three HEK293T GLIS2 TALEN lines (GFP.P2A.3xFLAG.GLIS2 FL (B), GFP.P2A.3xFLAG.GLIS2 1-121 (C) and GFP.P2A.3xFLAG.GLIS2 IVS5+1G>T (D)) versus the control line (GFP.P2A.3xFLAG). Ratios were plotted against the negative logarithmic P-value of the Student's t-test. Every detected protein is represented by a dot. Dots on the right side of the curved line are determined to be significant interactors (FDR 0.05, s0: 0,1). To **B** and **D**: Top 30 protein interactors (depicted in red) were chosen by multiplication of negative logarithmic P-value with log_2 fold change of LFQ value of one protein. The 30 proteins with the strongest interaction were marked in red (list of top interactors of GFP.P2A.3xFLAG.GLIS2 FL and GFP.P2A.3xFLAG.GLIS2 IVS5+1G>T in Table 2 A and C). To **C**: All significant interactors of GFP.P2A.3xFLAG.GLIS2 1-121 are depicted in red (table 2 B)

A

$-log_{10}$ p-value hGlis2-FL_Flag-Talen-IP_ctrl	**log_2 Difference hGlis2-FL_Flag-Talen-IP_ctrl**	**Protein IDs**	**Protein names**	**Gene names**
5,76243	4,18913	Q9UBI6	Guanine nucleotide-binding protein G(I)/G(S)/G(O) subunit gamma-12	GNG12
4,61137	3,82582	Q7Z2K8	G protein-regulated inducer of neurite outgrowth 1	GPRIN1
5,69428	3,08265	P08133	Annexin A6	ANXA6
6,70295	2,64513	P63096	Guanine nucleotide-binding protein G(i) subunit alpha-1	GNAI1
5,36267	3,08465	Q96BJ3	Axin interactor, dorsalization-associated protein	AIDA
5,45814	2,74595	Q9Y3L5	Ras-related protein Rap-2c	RAP2C
5,52982	2,70249	Q9NZR1	Tropomodulin-2	TMOD2
5,37231	2,7421	P13987	CD59 glycoprotein	CD59
4,77037	3,00529	Q15185	Prostaglandin E synthase 3	PTGES3
5,9628	2,27591	Q86X29	Lipolysis-stimulated lipoprotein receptor	LSR
5,1126	2,59373	Q9HAC8	Ubiquitin domain-containing protein 1	UBTD1
4,68196	2,75224	P49795	Regulator of G-protein signaling 19	RGS19
4,87865	2,60914	Q9Y2J2;Q9H4G0	Band 4.1-like protein 3;Band	EPB41L

			4.1-like protein 3, N-terminally processed	3
4,18699	3,034	P60953;P84095;P17081;Q9H4E5	Cell division control protein 42 homolog	CDC42
4,30492	2,76281	P07737;CON__P02584	Profilin-1	PFN1
5,16776	2,21384	P06396;REV__Q6TDU7	Gelsolin	GSN
4,2069	2,71697	Q14156	Protein EFR3 homolog A	EFR3A
3,37995	3,3537	Q9BR76;A9Z1Z3	Coronin-1B	CORO1B
4,10132	2,63791	P13591	Neural cell adhesion molecule 1	NCAM1
5,5974	1,91059	Q5TC63	Growth hormone-regulated TBC protein 1	GRTP1
4,64006	2,27557	Q9UKS6	Protein kinase C and casein kinase substrate in neurons protein 3	PACSIN3
4,70237	2,24237	O75369;Q14315	Filamin-B	FLNB
4,04302	2,60303	P19022;P55283	Cadherin-2	CDH2
5,81	1,81117	Q14152	Eukaryotic translation initiation factor 3 subunit A	EIF3A
4,09373	2,50408	Q12860	Contactin-1	CNTN1
5,17662	1,97426	Q9ULJ8	Neurabin-1	PPP1R9A
4,97748	2,05081	P04899	Guanine nucleotide-binding protein G(i) subunit alpha-2	GNAI2
5,54392	1,82769	Q09666;P48552	Neuroblast differentiation-associated protein AHNAK	AHNAK
3,77346	2,65904	Q0ZGT2	Nexilin	NEXN
4,63874	2,15844	P29966	Myristoylated alanine-rich C-kinase substrate	MARCKS

B

$-log_{10}$ p-value hGlis2-1-121_Flag-Talen-IP_ctrl	log_2 Difference hGlis2-1-121_Flag-Talen-IP_ctrl	Protein IDs	Protein names	Gene names
2,02623865	3,4113369	O14974	Protein phosphatase 1 regulatory subunit 12A	PPP1R12A
2,48987428	2,31237984	Q9Y5S2	Serine/threonine-protein kinase MRCK beta	CDC42BPB
2,17409814	2,21441317	P23470	Receptor-type tyrosine-protein	PTPRG

			phosphatase gamma	
2,16176653	2,22058249	P54826	Growth arrest-specific protein 1	GAS1
2,76640358	1,70435905	P49795	Regulator of G-protein signaling 19	RGS19
2,29867838	1,95638847	P13987	CD59 glycoprotein	CD59
2,29553561	1,89747715	P25787	Proteasome subunit alpha type-2	PSMA2
2,25924379	1,89570856	P09493	Tropomyosin alpha-1 chain	TPM1
2,9847833	1,39995193	Q96GA3	Protein LTV1 homolog	LTV1
2,31302462	1,76951408	Q9P0K7;Q9C0D0	Ankycorbin	RAI14
2,46491658	1,62725639	Q4VCS5;Q8IY63	Angiomotin	AMOT
2,40443223	1,6631732	P62191	26S protease regulatory subunit 4	PSMC1
2,26484368	1,51733303	P78368	Casein kinase I isoform gamma-2	CSNK1G2
3,56243759	0,66585922	P34932	Heat shock 70 kDa protein 4	HSPA4

C

$-log_{10}$ p-value hGlis2-(IVS5+1G>T)_Flag-Talen-IP_ctrl	**log_2 Difference hGlis2-(IVS5+1G>T)_Flag-Talen-IP_ctrl**	**Protein IDs**	**Protein names**	**Gene names**
4,41642204	4,84759331	Q9UBI6	Guanine nucleotide-binding protein G(I)/G(S)/G(O) subunit gamma-12	GNG12
5,9517704	3,01072741	Q9HAC8	Ubiquitin domain-containing protein 1	UBTD1
5,32801248	3,25308657	Q96BJ3	Axin interactor, dorsalization-associated protein	AIDA
6,68241355	2,56146288	P42356;A4QPH2;Q8N8J0	Phosphatidylinositol 4-kinase alpha	PI4KA
4,48484873	3,77360535	Q7Z2K8	G protein-regulated inducer of neurite outgrowth 1	GPRIN1
5,08223707	3,15878677	P19086	Guanine nucleotide-binding protein G(z) subunit alpha	GANZ
5,14129378	3,1163969	P19022;P55283	Cadherin-2	CDH2
5,8159554	2,73722887	Q86X29	Lipolysis-stimulated lipoprotein receptor	LSR

5,27131094	2,98893547	P13987	CD59 glycoprotein	CD59
6,51243974	2,35833549	P63096	Guanine nucleotide-binding protein G(i) subunit alpha-1	GNAI1
6,2091256	2,44550705	P29992;O95837	Guanine nucleotide-binding protein subunit alpha-11	GNA11
5,74903412	2,59295034	Q9Y3L5	Ras-related protein Rap-2c	RAP2C
5,17688421	2,86677837	P63000;P60763;P15153	Ras-related C3 botulinum toxin substrate 1;Ras-related C3 botulinum toxin substrate 3;Ras-related C3 botulinum toxin substrate 2	RAC1; RAC3; RAC2
5,78074396	2,56538773	P61225	Ras-related protein Rap-2b	RAP2B
4,46393525	3,23396826	Q14156	Protein EFR3 homolog A	EFR3A
6,71765403	2,13004541	Q14152	Eukaryotic translation initiation factor 3 subunit A	EIF3A
4,9701772	2,86534786	Q9Y2J2;Q9H4G0	Band 4.1-like protein 3;Band 4.1-like protein 3, N-terminally processed	EPB41L3
5,7261928	2,45419693	Q09666;P48552	Neuroblast differentiation-associated protein AHNAK	AHNAK
5,83075507	2,39995861	O75369;Q14315	Filamin-B	FLNB
4,28509871	3,25619984	P01112	GTPase HRas;GTPase HRas, N-terminally processed	HRAS
5,31433452	2,61180544	P06396;REV__Q6TDU7	Gelsolin	GSN
5,06842042	2,68973684	Q9NZR1	Tropomodulin-2	TMOD2
4,73983976	2,82629108	P08133	Annexin A6	ANXA6
4,56724917	2,90123701	Q86UN3	Reticulon-4 receptor-like 2	RTN4RL2
4,91954238	2,68500853	Q12860	Contactin-1	CNTN1
5,64999068	2,33410358	P04899	Guanine nucleotide-binding protein G(i) subunit alpha-2	GNAI2
4,98168267	2,64010715	O00161	Synaptosomal-associated protein 23	SNAP23
4,38588779	2,96822882	Q7L7X3	Serine/threonine-protein kinase TAO1	TAOK1
5,58921363	2,3150835	Q12904	Aminoacyl tRNA synthase complex-interacting	AIMP1

			multifunctional protein 1;Endothelial monocyte-activating polypeptide 2	
4,92447068	2,60756683	Q9Y6M4;Q9HCP0	Casein kinase I isoform gamma-3;Casein kinase I isoform gamma-1	CSNK1G3; CSNK1G1

Table 2: Top GLIS2 interactors of each TALEN cell line

A-C Tables of top interactors of each TALEN cell line. Top 30 interactors listed for 3xFLAG.GLIS2 FL (A) and 3xFLAG.GLIS2 IVS5+1G>T (C). 3xFLAG.GLIS2 1-121 (B) had only 14 significant interactors.

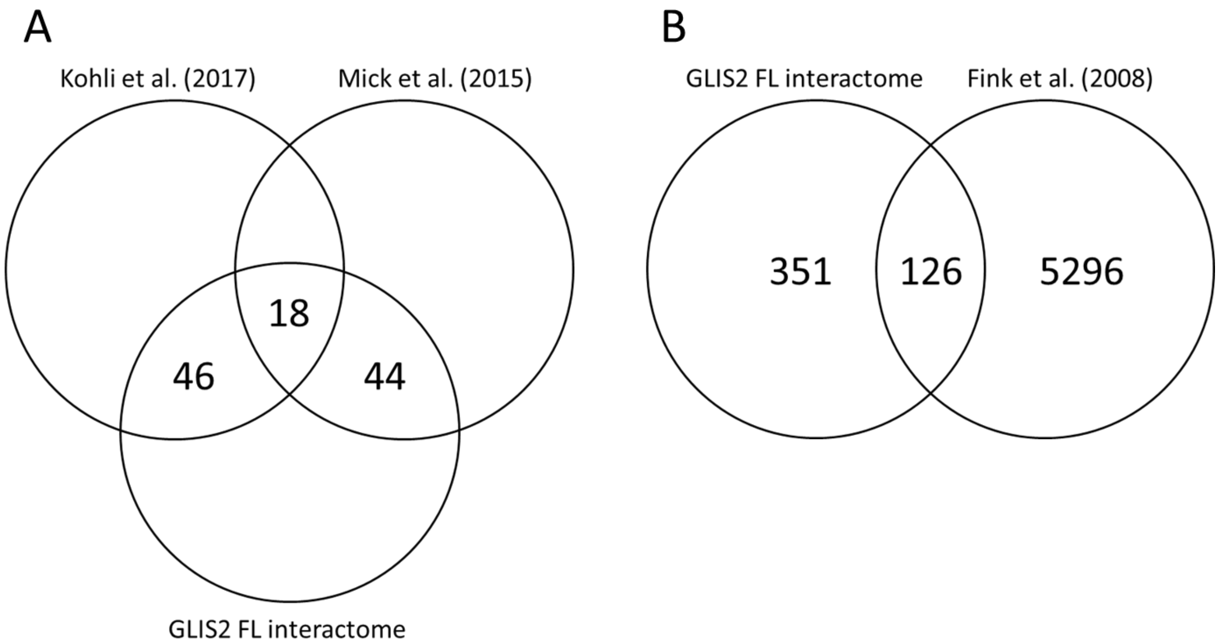

Fig. 6: Overlap of significant interactors (for GLIS2 FL) with ciliary and nuclear proteomes

A Venn diagram shows the overlap between significant interactors of 3xFLAG.GLIS2 FL and published ciliary proteomes. A list of ciliary proteins which are among the significant interactors of 3xFLAG.GLIS2 FL can be found in the supplements (section 7.4.) **B** Venn diagram showing the overlap between significant interactors of 3x.FLAG.GLIS2 FL and a nuclear proteome published by Fink et *al.* in 2008 [41].

$-log_{10}$ p-value hGlis2-FL_Flag-Talen-IP_ctrl	**log_2 Difference hGlis2-FL_Flag-Talen-IP_ctrl**	**Protein IDs**	**Protein names**	**Gene names**
2,26658838	0,38308716	P78527	DNA-dependent protein kinase catalytic subunit	PRKDC
1,35425931	0,32524395	Q92878	DNA repair protein RAD50	RAD50
2,58362698	0,44077206	P49916	DNA ligase 3	LIG3
2,37411254	0,46092415	P09874	Poly [ADP-ribose] polymerase 1	PARP1
1,34678916	1,25885582	P28340	DNA polymerase delta catalytic subunit	POLD1
3,44963628	0,66652918	P12956	X-ray repair cross-complementing protein 6 (Ku70)	XRCC6
3,02976583	0,75647402	P13010	X-ray repair cross-complementing protein 5 (Ku80)	XRCC5
4,90488816	1,91962051	P23921	Ribonucleoside-diphosphate reductase large subunit	RRM1

Table 3: **Central DDR proteins among the significant interactors of 3x.FLAG.GLIS2 FL**

5. Discussion

We aimed to study the physiological functions of GLIS2, and therefore several attempts were made to isolate GLIS2 for further analysis. The validation of a commercial anti-GLIS2 antibody revealed that this polyclonal antibody was not suitable for immunoprecipitation of endogenous or overexpressed GLIS2. The consecutive attempt to produce a homemade antibody by hybridoma culture was also not successful (section 4.1.). The approach to generate an IMCD3 3xFLAG-emGFP-KI GLIS2 CRISPR line worked methodically but was not suitable for any of the desired downstream applications due to the low expression of 3xFLAG.GLIS2 (section 4.2.).

The methodical difficulties of developing tools to investigate GLIS2's physiological functions are also discussed in this chapter (sections 5.1. and 5.2.), and alternative approaches for future experiments are pointed out.

The interactome of GLIS2 generated by mass spectrometry-based analysis of FLAG-immunoprecipitates of FLAG-tagged GLIS2 TALEN lines as described in this work provides the basis for future experiments elucidating the pathogenic mechanisms of NPH (type 7) and gives indications which role GLIS2 might play in the nucleus and potentially at the primary cilium (sections 5.3., 5.4. and 5.5.).

5.1. Challenges of anti-GLIS2 antibody generation by hybridoma culture and related techniques

The generation of monoclonal antibodies by hybridoma cell culture is a well-established method in the Nephrolab Cologne. The workflow for screening of hybridoma clones consisting of ELISA, western blot using a multi-blot-devise, immunofluorescence staining, and immunoprecipitation is also well-established. A crucial aspect regarding this screening workflow is that positive results in the ELISA (meaning high absorption values, section 3.11.) have only limited predictive worth. Thus, clones which had a strongly positive result in the ELISA were not suitable for immunofluorescence staining or immunoprecipitation, although, in all three techniques, the recognition of native protein is required. This observation might be due to different requirements regarding the affinity of a specific monoclonal antibody to its antigen between the different techniques, as the biochemical context in which the binding of the antibody to its antigen occurs is slightly different (see method section). Another aspect that limits the number of screened clones is that the ELISA, which is the first step in the screening workflow, selects for monoclonal antibodies with specificity for continuous or discontinuous epitopes, which need to be at the surface of the protein [51]. In contrast, in SDS-PAGE and immune blotting, a protein exists in its denatured state, thus lacking most of the discontinuous epitopes theoretically but presenting continuous epitopes, which are hardly accessible in the native state of the protein. This implies that monoclonal antibodies, which are not able to detect native protein (negative result in ELISA), still can have the potential to detect denatured protein by recognition of continuous epitopes, which are only accessible in the denatured state. This limitation of the workflow was accepted as the desired monoclonal anti-GLIS2 antibody should combine both requirements (recognition of native and denatured GLIS2) to be suitable for downstream applications, which require an immunoprecipitation step (ChIP-Seq, interactome analysis), and for western blot.

Another aspect to be considered is that the tertiary structure of the injected His-tagged GLIS2 (1-120 aa) peptide used for immunization might differ from this part of GLIS2 in the context of the wild-type protein due to steric interactions with other parts of GLIS2, which were not present in the injected peptide.

Another complication could be the generation of an anti-mouse-GLIS2 antibody by immunization of mice with His.GLIS2 (1-120 aa) of mouse origin. Potentially, the immunogenicity is reduced since the injected peptide is derived from the mouse homolog of GLIS2. This reduction might be due to the process of self-peptide presentation, which occurs continuously in eukaryotic cells, where proteins are degraded by the proteasome and the resulting peptide fragments are loaded on the major histocompatibility complex 1 (MHC1) (presents peptides with a length of 9-10 amino acids) and are presented on the cell surface to different cells of the immune system [140]. Several mechanisms prevent the activation of immune cells through these peptides [100]. The failure of these mechanisms can lead to auto-immune responses [100]. In summary, the immune response in the mouse evoked by a mouse peptide should be lower than the one evoked by a peptide derived from the homolog of another species. This might explain at least partially why the generation of an anti-GLIS2 antibody failed.

There is also an alternative way of processing hybridoma cells after fusion, which introduces an additional selection step based on the affinity of membrane-bound antibodies to the peptide the mouse was immunized with [119]. Special myeloma cells are used (so-called SP2ab cells) as fusion partners of the murine B-cells [119]. After fusion with PEG, the resulting hybridoma cells are able to secrete an antibody of certain specificity like conventional hybridoma cells but also to express a membrane-bound variant of the same antibody [119]. Thus, it is possible to incubate all the hybridoma cells resulting from the fusion with a fluorophore-coupled variant of the peptide, which was used for the immunization of the mouse [119]. Next, the cells are FAC-sorted [119]. In this way, only hybridoma cells that can bind the fluorophore-coupled peptide through their membrane-bound antibody have a positive fluorescence signal and are FAC-sorted accordingly [119]. This strategy would add a selection step to the workflow and would already select for hybridoma cells with specificity for native immunization peptides (e.g., His.mGLIS2 (1-120 aa)).

5.2. CRISPR/Cas9-based genome editing for generation of a monoclonal cell line

The generation of the monoclonal IMCD3 3xFLAG-emGFP-KI GLIS2 CRISPR line bypassed the problem of a missing anti-GLIS2 antibody. The CRISPR/Cas9 genome-editing system provides a new possibility to generate transgenic cell lines or organisms in an exact and flexible way [124]. As the endogenous copies of *Glis2* are tagged, the resulting cell line has very similar physiology compared to the wild-type cells [124]. In the case of overexpression or genome editing approaches, where a third copy of the gene encoding for a specific protein is introduced (e.g., TALEN), the amount of respective protein is typically higher as compared to the wild-type cell line [76]. Furthermore, the additional protein is transcribed from the coding sequence of the gene, which is under the control of a different promotor (in most cases, a promotor with high activity) [76]. As already described in the result section, the generated IMCD3 3xFLAG-emGFP-KI GLIS2 CRISPR line expressed a very low amount of 3xFLAG.emGFP.GLIS2, which made this cell line unsuitable for any of the desired downstream applications. This was due to the heterozygosity and most likely the extremely low physiologic expression level of GLIS2. However, the extremely low expression levels of GLIS2 could also have additional reasons. For example, GLIS2 might need a specific stimulus that upregulates its expression or induces its stabilization by post-translational modifications, which protects GLIS2 from degradation. Based on the hypothesis that GLIS2 plays a role in the DDR, a possible stimulus for GLIS2 expression or GLIS2 stabilization could be treatment with UV light or substances like aphidicolin which induces DNA damage and thus an increase in DDR signaling [135]. The problem of low expression levels could perhaps be solved by using a homozygous knock-in line, which might express higher levels of tagged GLIS2 per cell. At this point, the size (1287 bp) of the insert, which should be integrated into the genome, and the consecutive need to deliver the insert embedded in a plasmid, is critical and might have prevented homozygous integration. The strategy we used could be modified regarding the size of the insert. The sequence of the blasticidin resistance gene and the sequence of the adjacent P2A-peptide were actually not needed as the selection of transfected cells was based on FAC-sorting of GFP-positive cells (section 4.2.). The blasticidin resistance gene was introduced to the cells as a backup strategy for the selection of successfully transfected cells. Another way to shorten the insert would be to reduce the size of a tag sequence (e.g., 3xFLAG-tag only). Smaller inserts (up to 150 bp) offer the opportunity to be delivered in the form of cheap single-stranded oligodeoxynucleotides (ssODNs), which increases the probability of integration events [2]. More integration events would also lead to a higher number of transgenic cells from one transfection and also to a consecutive higher probability of homozygous transgenic cells, which might solve the problem of low levels of tagged GLIS2. However, even homozygous integration might not solve detection problems of endogenously-tagged proteins in the case of an extremely low abundant protein. In our case, however, we used TALEN-mediated integration of the transgene in a safe-harbor locus to continue with the GLIS2-interactome project.

5.3. Novel protein interactors of GLIS2 identified by MS-analysis and their possible relevance in the physiological context

The newly-generated dataset of significant protein interactors of GLIS2 derived from FLAG-immunoprecipitations of lysates from polyclonal stable cell lines, expressing wild-type GLIS2 and two GLIS2 truncations, is the first unbiased interactome for GLIS2 on the protein level. Other studies identified GLIS2 protein interactors by *yeast two-hybrid* (Y2H) screenings or co-immunoprecipitation experiments with overexpressed GLIS2 and prospective interactors in overexpression [72,122]. The risk of studying GLIS2 by using transient transfections is that this results in much higher expression levels when compared to endogenous levels and concomitant possible unspecific interactions with other proteins leading to false-positive results. We avoided this by using TALEN-mediated single copy integration. Limitations of the approach chosen in this work are that a stable cell line instead of kidney tissue was used and that the tagged GLIS2 protein is expressed under a different promotor as compared to endogenous GLIS2.

The mass spectrometry-based analysis of an immunoprecipitation has the theoretical potential to detect all proteins involved in a particular protein complex. This potential implicates the ability to additionally reveal proteins that are not directly interacting with GLIS2 but are also part of the same protein complex. Furthermore, it is vital to consider that volatile interactions between two proteins might not be detected since their interaction is only present shortly, at low affinity or because it only occurs in a particular cellular context (e.g., in the presence of a specific extracellular stimulus). Proteins expressed at low levels might not be detected and therefore missed in our analysis.

Among the 477 potential interactors, there are a few candidates who point into a whole new direction regarding the physiological functions of GLIS2. Remarkably, proteins like PARP1, DNA-PK (catalytic subunit), and RAD50 are critical players in the DNA damage response and are also part of the proteins complex that was determined as significant interactors of GLIS2 [25]. Especially, PARP1, DNA-PKcs, Ku70 (XRCC6), and

Ku80 (XRCC5) are involved in the recognition of DNA breaks and consecutive recruitment of downstream proteins of the DNA damage response signaling cascades [105]. RAD50 is also involved in DSB repair as it is part of the DSB-sensing MRN complex [16]. As described in the introduction (section 2.5.), seven NPH proteins (CEP164, GLIS2, ZNF423, NEK8, CEP290, SDCCAG8, MAPKBP1) have already been linked to DDR signaling, thereby creating a possible connection of altered or impaired DDR in the disease status and the resulting NPH phenotype [3,19,24,98,102,133]. Lu *et al.* (2016) showed that renal epithelial GLIS2 knock-out cells exhibit elevated levels of the DNA damage marker γH2AX (phosphorylated histone H2AX at Ser139), indicating that DNA damage-induced signaling is activated when GLIS2 function is impaired [98]. As the phosphorylation of H2AX is a reaction to a detected DNA lesion, this could implicate the accumulation of DNA damage in those cells in case the repair is insufficient. The interactome analysis presented in this work gives first hints for the possible mechanism underlying elevated levels of the DNA damage marker γH2AX. Therefore, it would be possible that GLIS2 represents an enhancer for critical components of the DDR like PARP1, DNA-PK, RAD50, Ku70, and Ku80, resulting in the prevention of the accumulation of DNA damage, thus preventing the cell from entering cellular processes like apoptosis or senescence [16]. The mechanistic connection between the accumulation of DNA damage and development of fibrosis with the epithelial-mesenchymal transition (EMT) as a central process on the one hand and inflammatory infiltration of the interstitium, on the other hand, remains to be uncovered for the context of NPH [7,98]. It is known that detecting DNA damage by components of the DDR like PARP1 or DNA-PK can stimulate interferon production with consecutive activation of the immune system [113]. For DNA-PK, this is only described in the context of cytoplasmic DNA, but for PARP1, NF-κB mediated transcription of TNF-α, IL-6, and iNOS upon DNA strand breaks of genomic DNA via activation of PIASy, NEMO, and ATM is described [105,113]. This mechanism represents a direct connection between DNA damage, as a result of genotoxic stress, replication stress, or inflammation. Furthermore, it is known that chronic inflammation promotes a profibrotic environment in the kidney, thereby promoting processes like EMT and profibrotic signaling, which further amplifies the genotoxic stress for the resident tissue cells [113]. This results in an accumulation of DNA damage and consecutively in an aggravation of the inflammatory response like a vicious circle, providing a pathophysiologic mechanism connecting impaired GLIS2 function and the resulting NPH phenotype [113].

The interactome of the cell line, expressing 3xFLAG GLIS2 (IVS5+1G>T), revealed 450 significant protein interactors, of which 412 protein interactor overlap with the full-length interactome (section 4.4.). This number is surprisingly high as this cell line was supposed to represent the mutant GLIS2 protein being present in patients with the IVS5+1G>T mutation. This result suggests that the postulated GLIS2 variant present in the TALEN line might be a different one than being present in the patients with NPH type 7. This assumption is further supported when looking into the mutant interactome as it contains, amongst others, the central DDR proteins like PARP1, DNA-PKcs, and RAD50. These are highly interesting protein interactors that also appear in the full-length interactome. The potential GLIS2 functions associated with these protein interactions could have an important pathogenic role in the pathophysiology of NPH type 7. In the end, it is difficult to judge how realistic the mutant variant of GLIS2 might be as the protein interactions which are crucial for GLIS2 function in the physiological context are not known yet.

The second mutant GLIS2 interactome derived from the cell line, expressing 3xFLAG.GLIS2 1-121, revealed 14 significant protein interactors (Figure 5 C; Table 2 B). This result reflects the fact that this GLIS2 truncation misses all five zinc finger domains, which are crucial for GLIS2 function and which are also required for the import of GLIS2 in the nucleus (especially the first three zinc finger domains). The mutant GLIS2 variant only localizes to the cytosol and is not transported into the nucleus, which was examined by immunofluorescence microscopy (section 4.3.). The mutant GLIS2 protein might be rapidly degraded in the cell because of its poor or missing functionality. The importance of the zinc finger domains for GLIS2 function is further underpinned by a recently reported patient mutation – an in-frame deletion of five amino acids – resulting in an altered structure of the first zinc finger domain, which was found to be causative for the typical NPH phenotype [4].

5.4. The question of subcellular localization of GLIS2 and respective functions

The GLIS2 interactome analysis potentially provides new insights regarding the subcellular localization of GLIS2 and the possible physiological functions of GLIS2 arising from the respective subcellular localization. NPH is classified as a ciliopathy as the gene products of the NPH-associated genes are all shown or at least thought to localize to the primary cilium. In the case of mutated GLIS2, which is responsible for NPH type 7, it is not yet clearly proven that GLIS2 localizes to the primary cilium. Attanasio *et al.* (2007) showed GLIS2 to localize to the primary cilium with distribution over the whole ciliary compartment [7]. In our lab, it was not possible to reproduce these results with the same antibody which was used for this publication and even with different overexpression constructs. A contradictory aspect for its localization in the ciliary compartment distal of the ciliary transition zone might be that GLIS2 lacks the ciliary localization signal (CLS), which is required for Transportin 1 (TNPO1) mediated import into the ciliary compartment [73]. Its paralogs GLIS3, GLI1, GLI2, and GLI3 use this mechanism to enter the ciliary compartment [73]. So if GLIS2 would localize to the primary cilium, one would expect it to localize rather at the ciliary base proximal of the transition zone. Nevertheless, TNPO1 is one of the significant interactors of GLIS2 revealed by the interactome analysis of GLIS2. This interaction could occur if GLIS2 localizes closely to the base of the primary cilium. Further evidence for this could be given by other significant interactors like Septin 2, 6, 7, and 11, which are localizing to the ciliary base [48,67,81,109]. As already described in the result section, the interactome analysis revealed some significant interactors of GLIS2 whose localization to the primary cilium was uncovered by analysis of the ciliary proteome in studies of Kohli *et al.* (2017) and Mick *et al.* (2015) [88,108]. Especially the group of 18 proteins (Fig. 6 A) detected in both ciliary proteomes, and the GLIS2 interactome is surprisingly large, providing further evidence for a ciliary localization of GLIS2. However, it is important to note that localization of most of these proteins is not completely specific for the ciliary compartment and they are also found in other cellular compartments. Nevertheless, this particular subset of GLIS2 interactors can provide the basis for future studies targeting the question of the physiological functions of GLIS2 at the primary cilium.

The dataset of significant interactors of GLIS2 also contains many actin-associated proteins and actin components like Alpha-actinin 1 and 4 (ACTN1 and ACTN4), cell division control protein 42 homolog (CDC42), Myosin 9 (MYO9), Myosin 10 (MYO10), Myosin 14 (MYO14), Src substrate cortactin (CTTN), Gelsolin (GSN), Dynactin subunit 1 and 2 (DCTN1 and DCTN2), Tropomyosin alpha-1,-3 and -4 (TPM1, TPM3, and TRM4)). The GO-term enrichment analysis regarding biological processes also yielded terms like "positive regulation of actin filament bundle assembly". Taken together, these results could raise the hypothesis that GLIS2 plays a role in the regulation of ciliary processes through actin regulation. Currently, the functional relation between primary cilia and actin regulation is assumed to work in an antagonistic way, meaning that actin polymerization results in ciliary disassembly, and depolymerization of actin results in the formation of the primary cilium [109]. Furthermore, there is a functional coupling between cilia formation and cell cycle progression, which consists in the presence of cilia in the G0/G1 phase, when the centriole is not needed as a spindle pole during mitosis [109,132]. Prior to mitosis, cilia are disassembled, and the centriole, which served as an anchor point for the microtubule-based scaffold of the primary cilium, can now perform its mitotic functions [109]. This functional connection requires signaling cascades, which transduce information about the cell cycle phase and nuclear processes to the ciliary compartment to trigger ciliogenesis or disassembly of primary cilia. The centriole is thought to play a crucial role as a signaling hub for orchestrating these signaling pathways [109]. Vice versa, information from external stimuli is transduced from the primary cilium into the nucleus to adapt the cell cycle and nuclear processes to the environment of the cell [104]. Thus, GLIS2 might be involved in the crosstalk between these two subcellular compartments as it might localize to the ciliary and nuclear compartment. This involvement could be facilitated through the regulation of the actin cytoskeleton. Especially the GLIS2 interactors, which are known to have a function in actin regulation and are also part of the ciliary proteome, might be attractive candidates for further studies regarding the function of GLIS2 on actin dynamics and thereby potentially regulating ciliary assembly or disassembly. Among this group of proteins, CDC42, GSN and CTTN are exciting candidates. CTTN is known to promote actin polymerization and thereby promotes ciliary disassembly in its phosphorylated status (phosphorylated by Src) and promotes cilia formation in its dephosphorylated status [109]. GSN is known to regulate cilia assembly positively [109]. CDC42 is known to regulate the cell cycle and regulate actin cytoskeleton and rearrangement [109].

Another interesting protein interactor of GLIS2, which was uncovered by the interactome analysis of this work and which was also predicted in advance by an algorithm called Scansite 4.0, is 14-3-3 protein theta (YWHAQ). This interactor is associated with a specific regulation mechanism that leads to the sequestration of a protein in a cellular compartment, thus preventing this protein from entering another cellular compartment. This has been described in the case of Hippo signaling, where 14-3-3 binds phosphorylated YAP/TAZ (transcription factor), thereby sequestering YAP/TAZ in the cytosol and inhibiting its translocation into the nucleus [86,149]. This might also be a mechanism for the regulation of nuclear GLIS2 functions in response to signaling cascades starting from the ciliary compartment.

5.5. Hypothesis and outlook

As discussed above, the novel GLIS2 interactome provides a new basis for future studies targeting the function of GLIS2 to understand the underlying mechanisms leading to NPH type 7 in case of mutations of GLIS2. The identification of central proteins involved in DNA damage response as significant interactors (Table 3) supports the hypothesis that GLIS2 might function as a DNA damage response player, which is of particular importance for tissues with a high level of genotoxic stress like the kidney [19]. In case GLIS2 function is impaired, accumulation of DNA damage in those cells might evoke a response of the innate immune system through sensing the DSBs by PARP1, which leads to consecutive transcription and secretion of profibrotic factors (via NFκB activation). In this way, a status of chronic inflammation and a profibrotic environment could be established, which promotes excessive fibrosis, which is the histopathologic key feature of NPH [132]. To prove this hypothesis, a validation of the mentioned interactors by co-immunoprecipitation and detailed analysis of *Glis2* knock-out mice concerning this hypothesis would be a possible approach.

Besides revealing the impact of nuclear functions of GLIS2 on the development of NPH, the ciliary localization of GLIS2 still needs to be confirmed, and respective functions at the primary cilium to be characterized (validation of promising ciliary interactors by co-immunoprecipitation). As many ciliary proteins appeared in the GLIS2 interactome, this provides evidence for ciliary localization of GLIS2. The predominance of axonemal and centrosomal proteins among the GLIS2 interactors, together with the absence of the CLS sequence in the GLIS2 amino acid sequence, suggest that GLIS2 might rather localize to the ciliary base. Actin regulatory proteins among the group of interactors that are also part of the ciliary proteome raise the hypothesis that GLIS2 could be involved in the regulation of actin dynamics, thereby regulating ciliary assembly or disassembly [109]. In this respect, it would be interesting to look at the architecture of the actin cytoskeleton (especially the part of the cortical actin cytoskeleton around the base of the primary cilium) in wild-type cells (e.g., IMCD3 cells) or in a wild-type mouse kidney compared to GLIS2 deficient cells or mice and to validate the interaction between GLIS2 and the most important actin regulatory proteins of the GLIS2 interactome via co-immunoprecipitation. Taking these findings together, a model of a dual role of GLIS2 with nuclear and ciliary localization enabling the coordination of nuclear and ciliary processes would be the consequence. If GLIS2 localizes to the primary cilium, it would also be interesting to investigate whether shuttling of GLIS2 between the nucleus and the primary cilium occurs. An exciting aspect about the research which has been done on GLIS2 so far is that all biochemical analysis of GLIS2 functions, its interactions with other proteins, and its subcellular localization was never done with endogenous GLIS2 [7,66,80,83,84,98,121-123,145,151,152]. An exception is the immunofluorescence staining of MDCK-II cells with a homemade anti-GLIS2 antibody in the publication of Attanasio *et al.* (2007), which was not reproducible in our lab [7]. In combination with our difficulties to develop tools for the biochemical analysis of endogenous GLIS2, like the generation of a homemade anti-GLIS2 antibody by hybridoma culture, one could think of other possibilities than a protein that is transcribed from the *GLIS2* locus. The NPH phenotype observed in patients having a mutation in the *GLIS2* gene on both alleles or in *Glis2* knock-out mice could also be caused by disruption of a regulative RNA transcribed from the *Glis2* gene. There are candidates of possible circular RNA transcripts, which would also explain the NPH phenotype in the generated *Glis2* knock-out mice and the patients with NPH type 7 [7,83].

Of course, this is a speculative hypothesis but highly interesting and potentially worth following up.

6. Literature

1. Adan A, Alizada G, Kiraz Y, Baran Y, Nalbant A. Flow cytometry: basic principles and applications. *Critical reviews in biotechnology* 2017; **37**(2): 163-76.
2. Aird EJ, Lovendahl KN, St. Martin A, Harris RS, Gordon WR. Increasing Cas9-mediated homology-directed repair efficiency through covalent tethering of DNA repair template. *Communications Biology* 2018; **1**(1): 54.
3. Airik R, Slaats G, Guo Z, Weiss A-C, Khan N, Ghosh A, Hurd T, Bekker-Jensen S, Schrøder J, J Elledge S, S Andersen J, Kispert A, Castelli M, Boletta A, Giles R, Hildebrandt F. Renal-Retinal Ciliopathy Gene Sdccag8 Regulates DNA Damage Response Signaling; 2014.
4. Al Alawi I, Powell L, Rice SJ, Al Riyami MS, Al-Riyami M, Al Salmi I, Sayer JA. Case Report: A Novel In-Frame Deletion of GLIS2 Leading to Nephronophthisis and Early Onset Kidney Failure. *Frontiers in genetics* 2021; **12**: 791495.
5. Arquint C, Gabryjonczyk A-M, Nigg EA. Centrosomes as signalling centres. *Philosophical transactions of the Royal Society of London Series B, Biological sciences* 2014; **369**(1650): 20130464.
6. Arts HH, Knoers NVAM. Current insights into renal ciliopathies: what can genetics teach us? *Pediatric nephrology (Berlin, Germany)* 2013; **28**(6): 863-74.
7. Attanasio M, Uhlenhaut NH, Sousa VH, O'Toole JF, Otto E, Anlag K, Klugmann C, Treier AC, Helou J, Sayer JA, Seelow D, Nurnberg G, Becker C, Chudley AE, Nurnberg P, Hildebrandt F, Treier M. Loss of GLIS2 causes nephronophthisis in humans and mice by increased apoptosis and fibrosis. *Nature genetics* 2007; **39**(8): 1018-24.
8. Avis KE, Levchuk JW. Special considerations in the use of vertical laminar-flow workbenches. *American journal of hospital pharmacy* 1984; **41**(1): 81-7.
9. Awata J, Takada S, Standley C, Lechtreck KF, Bellvé KD, Pazour GJ, Fogarty KE, Witman GB. NPHP4 controls ciliary trafficking of membrane proteins and large soluble proteins at the transition zone. *Journal of cell science* 2014; **127**(21): 4714-27.
10. Aydin S. A short history, principles, and types of ELISA, and our laboratory experience with peptide/protein analyses using ELISA. *Peptides* 2015; **72**: 4-15.
11. Bae KT, Zhu F, Chapman AB, Torres VE, Grantham JJ, Guay-Woodford LM, Baumgarten DA, King BF, Jr., Wetzel LH, Kenney PJ, Brummer ME, Bennett WM, Klahr S, Meyers CM, Zhang X, Thompson PA, Miller JP. Magnetic resonance imaging evaluation of hepatic cysts in early autosomal-dominant polycystic kidney disease: the Consortium for Radiologic Imaging Studies of Polycystic Kidney Disease cohort. *Clinical journal of the American Society of Nephrology : CJASN* 2006; **1**(1): 64-9.
12. Bass JJ, Wilkinson DJ, Rankin D, Phillips BE, Szewczyk NJ, Smith K, Atherton PJ. An overview of technical considerations for Western blotting applications to physiological research. *Scand J Med Sci Sports* 2017; **27**(1): 4-25.
13. Bell PD, Fitzgibbon W, Sas K, Stenbit AE, Amria M, Houston A, Reichert R, Gilley S, Siegal GP, Bissler J, Bilgen M, Chou PC, Guay-Woodford L, Yoder B, Haycraft CJ, Siroky B. Loss of primary cilia upregulates renal hypertrophic signaling and promotes cystogenesis. *Journal of the American Society of Nephrology : JASN* 2011; **22**(5): 839-48.
14. Bergmann C. ARPKD and early manifestations of ADPKD: the original polycystic kidney disease and phenocopies. *Pediatric nephrology (Berlin, Germany)* 2015; **30**(1): 15-30.
15. Bisgrove BW, Yost HJ. The roles of cilia in developmental disorders and disease. *Development (Cambridge, England)* 2006; **133**(21): 4131-43.
16. Blackford AN, Jackson SP. ATM, ATR, and DNA-PK: The Trinity at the Heart of the DNA Damage Response. *Molecular Cell* 2017; **66**(6): 801-17.

17. Boehlke C, Kotsis F, Patel V, Braeg S, Voelker H, Bredt S, Beyer T, Janusch H, Hamann C, Godel M, Muller K, Herbst M, Hornung M, Doerken M, Kottgen M, Nitschke R, Igarashi P, Walz G, Kuehn EW. Primary cilia regulate mTORC1 activity and cell size through Lkb1. *Nature cell biology* 2010; **12**(11): 1115-22.
18. Bornhorst JA, Falke JJ. Purification of proteins using polyhistidine affinity tags. *Methods in enzymology* 2000; **326**: 245-54.
19. Chaki M, Airik R, Ghosh AK, Giles RH, Chen R, Slaats GG, Wang H, Hurd TW, Zhou W, Cluckey A, Gee HY, Ramaswami G, Hong CJ, Hamilton BA, Cervenka I, Ganji RS, Bryja V, Arts HH, van Reeuwijk J, Oud MM, Letteboer SJ, Roepman R, Husson H, Ibraghimov-Beskrovnaya O, Yasunaga T, Walz G, Eley L, Sayer JA, Schermer B, Liebau MC, Benzing T, Le Corre S, Drummond I, Janssen S, Allen SJ, Natarajan S, O'Toole JF, Attanasio M, Saunier S, Antignac C, Koenekoop RK, Ren H, Lopez I, Nayir A, Stoetzel C, Dollfus H, Massoudi R, Gleeson JG, Andreoli SP, Doherty DG, Lindstrad A, Golzio C, Katsanis N, Pape L, Abboud EB, Al-Rajhi AA, Lewis RA, Omran H, Lee EY, Wang S, Sekiguchi JM, Saunders R, Johnson CA, Garner E, Vanselow K, Andersen JS, Shlomai J, Nurnberg G, Nurnberg P, Levy S, Smogorzewska A, Otto EA, Hildebrandt F. Exome capture reveals ZNF423 and CEP164 mutations, linking renal ciliopathies to DNA damage response signaling. *Cell* 2012; **150**(3): 533-48.
20. Chapman AB, Devuyst O, Eckardt KU, Gansevoort RT, Harris T, Horie S, Kasiske BL, Odland D, Pei Y, Perrone RD, Pirson Y, Schrier RW, Torra R, Torres VE, Watnick T, Wheeler DC. Autosomal-dominant polycystic kidney disease (ADPKD): executive summary from a Kidney Disease: Improving Global Outcomes (KDIGO) Controversies Conference. *Kidney international* 2015; **88**(1): 17-27.
21. Chebib FT, Torres VE. Autosomal Dominant Polycystic Kidney Disease: Core Curriculum 2016. *American journal of kidney diseases : the official journal of the National Kidney Foundation* 2016; **67**(5): 792-810.
22. Chen C, Okayama H. High-efficiency transformation of mammalian cells by plasmid DNA. *Molecular and cellular biology* 1987; **7**(8): 2745-52.
23. Chen Y. Calcium Phosphate Transfection of Eukaryotic Cells. *Bio-protocol* 2012; **2**(3): e86.
24. Choi HJC, Lin J-R, Vannier J-B, Slaats GG, Kile AC, Paulsen RD, Manning DK, Beier DR, Giles RH, Boulton SJ, Cimprich KA. NEK8 links the ATR-regulated replication stress response and S phase CDK activity to renal ciliopathies. *Molecular cell* 2013; **51**(4): 423-39.
25. Ciccia A, Elledge SJ. The DNA Damage Response: Making It Safe to Play with Knives. *Molecular Cell* 2010; **40**(2): 179-204.
26. Cohen SN. DNA cloning: A personal view after 40 years. *Proceedings of the National Academy of Sciences* 2013; **110**(39): 15521.
27. Corbit KC, Aanstad P, Singla V, Norman AR, Stainier DY, Reiter JF. Vertebrate Smoothened functions at the primary cilium. *Nature* 2005; **437**(7061): 1018-21.
28. Cornec-Le Gall E, Alam A, Perrone RD. Autosomal dominant polycystic kidney disease. *The Lancet* 2019; **393**(10174): 919-35.
29. Cornec-Le Gall E, Torres VE, Harris PC. Genetic Complexity of Autosomal Dominant Polycystic Kidney and Liver Diseases. *Journal of the American Society of Nephrology : JASN* 2018; **29**(1): 13-23.
30. Cox J, Mann M. 1D and 2D annotation enrichment: a statistical method integrating quantitative proteomics with complementary high-throughput data. *BMC Bioinformatics* 2012; **13 Suppl 16**(Suppl 16): S12-S.
31. Cox J, Mann M. MaxQuant enables high peptide identification rates, individualized p.p.b.-range mass accuracies and proteome-wide protein quantification. *Nature Biotechnology* 2008; **26**: 1367.
32. Dana H, Chalbatani GM, Mahmoodzadeh H, Karimloo R, Rezaiean O, Moradzadeh A, Mehmandoost N, Moazzen F, Mazraeh A, Marmari V, Ebrahimi

M, Rashno MM, Abadi SJ, Gharagouzlo E. Molecular Mechanisms and Biological Functions of siRNA. *International journal of biomedical science : IJBS* 2017; **13**(2): 48-57.
33. Davenport JR, Yoder BK. An incredible decade for the primary cilium: a look at a once-forgotten organelle. *American journal of physiology Renal physiology* 2005; **289**(6): F1159-69.
34. DeCaen PG, Delling M, Vien TN, Clapham DE. Direct recording and molecular identification of the calcium channel of primary cilia. *Nature* 2013; **504**(7479): 315-8.
35. Delling M, DeCaen PG, Doerner JF, Febvay S, Clapham DE. Primary cilia are specialized calcium signalling organelles. *Nature* 2013; **504**(7479): 311-4.
36. Delling M, Indzhykulian AA, Liu X, Li Y, Xie T, Corey DP, Clapham DE. Primary cilia are not calcium-responsive mechanosensors. *Nature* 2016; **531**: 656.
37. Diener DR, Lupetti P, Rosenbaum JL. Proteomic analysis of isolated ciliary transition zones reveals the presence of ESCRT proteins. *Current biology : CB* 2015; **25**(3): 379-84.
38. Donaldson JG. Immunofluorescence staining. *Current protocols in cell biology* 2001; **Chapter 4**: Unit 4.3.
39. Falck J, Coates J, Jackson SP. Conserved modes of recruitment of ATM, ATR and DNA-PKcs to sites of DNA damage. *Nature* 2005; **434**(7033): 605-11.
40. Felgner PL, Gadek TR, Holm M, Roman R, Chan HW, Wenz M, Northrop JP, Ringold GM, Danielsen M. Lipofection: a highly efficient, lipid-mediated DNA-transfection procedure. *Proceedings of the National Academy of Sciences of the United States of America* 1987; **84**(21): 7413-7.
41. Fink JL, Karunaratne S, Mittal A, Gardiner DM, Hamilton N, Mahony D, Kai C, Suzuki H, Hayashizaki Y, Teasdale RD. Towards defining the nuclear proteome. *Genome Biology* 2008; **9**(1): R15.
42. Fletcher L, Muschel RJ. The centrosome and the DNA damage induced checkpoint. *Cancer letters* 2006; **243**(1): 1-8.
43. Fliegauf M, Benzing T, Omran H. When cilia go bad: cilia defects and ciliopathies. *Nature reviews Molecular cell biology* 2007; **8**(11): 880-93.
44. Garcia-Gonzalo FR, Reiter JF. Scoring a backstage pass: Mechanisms of ciliogenesis and ciliary access. *The Journal of cell biology* 2012; **197**(6): 697.
45. Garcia G, III, Raleigh DR, Reiter JF. How the Ciliary Membrane Is Organized Inside-Out to Communicate Outside-In. *Current Biology* 2018; **28**(8): R421-R34.
46. Garibyan L, Avashia N. Polymerase chain reaction. *J Invest Dermatol* 2013; **133**(3): 1-4.
47. Gerdes JM, Katsanis N. Ciliary function and Wnt signal modulation. *Current topics in developmental biology* 2008; **85**: 175-95.
48. Ghossoub R, Hu Q, Failler M, Rouyez MC, Spitzbarth B, Mostowy S, Wolfrum U, Saunier S, Cossart P, Jamesnelson W, Benmerah A. Septins 2, 7 and 9 and MAP4 colocalize along the axoneme in the primary cilium and control ciliary length. *Journal of cell science* 2013; **126**(Pt 12): 2583-94.
49. Gomez-Godinez V, Wu T, Sherman AJ, Lee CS, Liaw L-H, Zhongsheng Y, Yokomori K, Berns MW. Analysis of DNA double-strand break response and chromatin structure in mitosis using laser microirradiation. *Nucleic acids research* 2010; **38**(22): e202-e.
50. Goto H, Inaba H, Inagaki M. Mechanisms of ciliogenesis suppression in dividing cells. *Cellular and molecular life sciences : CMLS* 2017; **74**(5): 881-90.
51. Greenbaum J, Haste Andersen P, Blythe M, Bui H-H, Cachau R, Crowe J, Davies M, Kolaskar A, Lund O, Morrison S, Mumey B, Ofran Y, Pellequer J-L, Pinilla C, Ponomarenko J, Raghava G, Van Regenmortel M, Roggen E, Sette A, Peters B. Towards a consensus on datasets and evaluation metrics for developing B-cell epitope prediction tools; 2007.

52. Guay-Woodford LM. Autosomal recessive polycystic kidney disease: the prototype of the hepato-renal fibrocystic diseases. *J Pediatr Genet* 2014; **3**(2): 89-101.
53. Guay-Woodford LM, Bissler JJ, Braun MC, Bockenhauer D, Cadnapaphornchai MA, Dell KM, Kerecuk L, Liebau MC, Alonso-Peclet MH, Shneider B, Emre S, Heller T, Kamath BM, Murray KF, Moise K, Eichenwald EE, Evans J, Keller RL, Wilkins-Haug L, Bergmann C, Gunay-Aygun M, Hooper SR, Hardy KK, Hartung EA, Streisand R, Perrone R, Moxey-Mims M. Consensus expert recommendations for the diagnosis and management of autosomal recessive polycystic kidney disease: report of an international conference. *The Journal of pediatrics* 2014; **165**(3): 611-7.
54. Gültekin H, Heermann KH. The use of polyvinylidenedifluoride membranes as a general blotting matrix. *Analytical Biochemistry* 1988; **172**(2): 320-9.
55. Hains PG, Robinson PJ. The Impact of Commonly Used Alkylating Agents on Artifactual Peptide Modification. *Journal of proteome research* 2017; **16**(9): 3443-7.
56. Halbritter J, Porath JD, Diaz KA, Braun DA, Kohl S, Chaki M, Allen SJ, Soliman NA, Hildebrandt F, Otto EA, The GPNSG. Identification of 99 novel mutations in a worldwide cohort of 1,056 patients with a nephronophthisis-related ciliopathy. *Human Genetics* 2013; **132**(8): 865-84.
57. Heather JM, Chain B. The sequence of sequencers: The history of sequencing DNA. *Genomics* 2016; **107**(1): 1-8.
58. Hebia C, Bekale L, Chanphai P, Agbebavi J, Tajmir-Riahi HA. Trypsin inhibitor complexes with human and bovine serum albumins: TEM and spectroscopic analysis. *Journal of photochemistry and photobiology B, Biology* 2014; **130**: 254-9.
59. Hildebrandt F, Attanasio M, Otto E. Nephronophthisis: disease mechanisms of a ciliopathy. *Journal of the American Society of Nephrology : JASN* 2009; **20**(1): 23-35.
60. Hildebrandt F, Benzing T, Katsanis N. Ciliopathies. *New England Journal of Medicine* 2011; **364**(16): 1533-43.
61. Hille F, Richter H, Wong SP, Bratovic M, Ressel S, Charpentier E. The Biology of CRISPR-Cas: Backward and Forward. *Cell* 2018; **172**(6): 1239-59.
62. Hoenig MP, Zeidel ML. Homeostasis, the milieu interieur, and the wisdom of the nephron. *Clinical journal of the American Society of Nephrology : CJASN* 2014; **9**(7): 1272-81.
63. Hogan MC, Abebe K, Torres VE, Chapman AB, Bae KT, Tao C, Sun H, Perrone RD, Steinman TI, Braun W, Winklhofer FT, Miskulin DC, Rahbari-Oskoui F, Brosnahan G, Masoumi A, Karpov IO, Spillane S, Flessner M, Moore CG, Schrier RW. Liver involvement in early autosomal-dominant polycystic kidney disease. *Clinical gastroenterology and hepatology : the official clinical practice journal of the American Gastroenterological Association* 2015; **13**(1): 155-64.e6.
64. Holzlöhner P, Hanack K. Generation of Murine Monoclonal Antibodies by Hybridoma Technology. *J Vis Exp* 2017; (119): 54832.
65. Hoseini SS, Sauer MG. Molecular cloning using polymerase chain reaction, an educational guide for cellular engineering. *J Biol Eng* 2015; **9**: 2-.
66. Hosking CR, Ulloa F, Hogan C, Ferber EC, Figueroa A, Gevaert K, Birchmeier W, Briscoe J, Fujita Y. The transcriptional repressor Glis2 is a novel binding partner for p120 catenin. *Molecular biology of the cell* 2007; **18**(5): 1918-27.
67. Hu Q, Milenkovic L, Jin H, Scott MP, Nachury MV, Spiliotis ET, Nelson WJ. A septin diffusion barrier at the base of the primary cilium maintains ciliary membrane protein distribution. *Science (New York, NY)* 2010; **329**(5990): 436-9.
68. Huangfu D, Liu A, Rakeman AS, Murcia NS, Niswander L, Anderson KV. Hedgehog signalling in the mouse requires intraflagellar transport proteins. *Nature* 2003; **426**(6962): 83-7.

69. Hughes J, Ward CJ, Peral B, Aspinwall R, Clark K, San Millan JL, Gamble V, Harris PC. The polycystic kidney disease 1 (PKD1) gene encodes a novel protein with multiple cell recognition domains. *Nature genetics* 1995; **10**(2): 151-60.
70. Hussain H, Chong NF-M. Combined Overlap Extension PCR Method for Improved Site Directed Mutagenesis. *Biomed Res Int* 2016; **2016**: 8041532-.
71. Ishikawa H, Marshall WF. Intraflagellar Transport and Ciliary Dynamics. *Cold Spring Harbor perspectives in biology* 2017; **9**(3).
72. Ivanov AA, Gonzalez-Pecchi V, Khuri LF, Niu Q, Wang Y, Xu Y, Bai Y, Mo X, Prochownik EV, Johns MA, Du Y, Khuri FR, Fu H. OncoPPi-informed discovery of mitogen-activated protein kinase kinase 3 as a novel binding partner of c-Myc. *Oncogene* 2017; **36**(42): 5852-60.
73. Jetten AM. GLIS1-3 transcription factors: critical roles in the regulation of multiple physiological processes and diseases. *Cellular and molecular life sciences : CMLS* 2018; **75**(19): 3473-94.
74. Jiang L, Li L, Zhao C, Pang X-R, Shen Q, Chang W-S, Zhai J. Genetic and antigenic analysis of mink's immunoglobulin G Fc region. *Cent Eur J Immunol* 2014; **39**(1): 36-9.
75. Johnson CA, Collis SJ. Ciliogenesis and the DNA damage response: a stressful relationship. *Cilia* 2016; **5**: 19-.
76. Joung JK, Sander JD. TALENs: a widely applicable technology for targeted genome editing. *Nature reviews Molecular cell biology* 2013; **14**(1): 49-55.
77. Kagan KO, Dufke A, Gembruch U. Renal cystic disease and associated ciliopathies. *Current opinion in obstetrics & gynecology* 2017; **29**(2): 85-94.
78. Kerzendorfer C, O'Driscoll M. Human DNA damage response and repair deficiency syndromes: linking genomic instability and cell cycle checkpoint proficiency. *DNA repair* 2009; **8**(9): 1139-52.
79. Khan P, Idrees D, Moxley MA, Corbett JA, Ahmad F, von Figura G, Sly WS, Waheed A, Hassan MI. Luminol-based chemiluminescent signals: clinical and non-clinical application and future uses. *Appl Biochem Biotechnol* 2014; **173**(2): 333-55.
80. Kim SC, Kim YS, Jetten AM. Kruppel-like zinc finger protein Gli-similar 2 (Glis2) represses transcription through interaction with C-terminal binding protein 1 (CtBP1). *Nucleic acids research* 2005; **33**(21): 6805-15.
81. Kim SK, Shindo A, Park TJ, Oh EC, Ghosh S, Gray RS, Lewis RA, Johnson CA, Attie-Bittach T, Katsanis N, Wallingford JB. Planar cell polarity acts through septins to control collective cell movement and ciliogenesis. *Science (New York, NY)* 2010; **329**(5997): 1337-40.
82. Kim TK, Eberwine JH. Mammalian cell transfection: the present and the future. *Analytical and bioanalytical chemistry* 2010; **397**(8): 3173-8.
83. Kim YS, Kang HS, Herbert R, Beak JY, Collins JB, Grissom SF, Jetten AM. Kruppel-like zinc finger protein Glis2 is essential for the maintenance of normal renal functions. *Molecular and cellular biology* 2008; **28**(7): 2358-67.
84. Kim YS, Kang HS, Jetten AM. The Kruppel-like zinc finger protein Glis2 functions as a negative modulator of the Wnt/beta-catenin signaling pathway. *FEBS letters* 2007; **581**(5): 858-64.
85. Klatte T, Ficarra V, Gratzke C, Kaouk J, Kutikov A, Macchi V, Mottrie A, Porpiglia F, Porter J, Rogers CG, Russo P, Thompson RH, Uzzo RG, Wood CG, Gill IS. A Literature Review of Renal Surgical Anatomy and Surgical Strategies for Partial Nephrectomy. *European urology* 2015; **68**(6): 980-92.
86. Kleppe R, Martinez A, Doskeland SO, Haavik J. The 14-3-3 proteins in regulation of cellular metabolism. *Seminars in cell & developmental biology* 2011; **22**(7): 713-9.
87. Kohler G, Howe SC, Milstein C. Fusion between immunoglobulin-secreting and nonsecreting myeloma cell lines. *European journal of immunology* 1976; **6**(4): 292-5.

88. Kohli P, Hohne M, Jungst C, Bertsch S, Ebert LK, Schauss AC, Benzing T, Rinschen MM, Schermer B. The ciliary membrane-associated proteome reveals actin-binding proteins as key components of cilia. *EMBO reports* 2017; **18**(9): 1521-35.
89. Kopitko C, Medve L, Gondos T. PathoPhysiology of renal blood suPPly; 2016.
90. Kramer A, Mailand N, Lukas C, Syljuasen RG, Wilkinson CJ, Nigg EA, Bartek J, Lukas J. Centrosome-associated Chk1 prevents premature activation of cyclin-B-Cdk1 kinase. *Nature cell biology* 2004; **6**(9): 884-91.
91. Lanktree MB, Haghighi A, Guiard E, Iliuta IA, Song X, Harris PC, Paterson AD, Pei Y. Prevalence Estimates of Polycystic Kidney and Liver Disease by Population Sequencing. *Journal of the American Society of Nephrology : JASN* 2018; **29**(10): 2593-600.
92. Lee JJ, von Kessler DP, Parks S, Beachy PA. Secretion and localized transcription suggest a role in positional signaling for products of the segmentation gene hedgehog. *Cell* 1992; **71**(1): 33-50.
93. Lee PY, Costumbrado J, Hsu C-Y, Kim YH. Agarose gel electrophoresis for the separation of DNA fragments. *J Vis Exp* 2012; (62): 3923.
94. Li B, Rauhauser AA, Dai J, Sakthivel R, Igarashi P, Jetten AM, Attanasio M. Increased hedgehog signaling in postnatal kidney results in aberrant activation of nephron developmental programs. *Human molecular genetics* 2011; **20**(21): 4155-66.
95. Liu JKH. The history of monoclonal antibody development - Progress, remaining challenges and future innovations. *Ann Med Surg (Lond)* 2014; **3**(4): 113-6.
96. Liu Z, Chen O, Wall JBJ, Zheng M, Zhou Y, Wang L, Ruth Vaseghi H, Qian L, Liu J. Systematic comparison of 2A peptides for cloning multi-genes in a polycistronic vector. *Scientific reports* 2017; **7**(1): 2193-.
97. Loenen WAM, Dryden DTF, Raleigh EA, Wilson GG, Murray NE. Highlights of the DNA cutters: a short history of the restriction enzymes. *Nucleic acids research* 2014; **42**(1): 3-19.
98. Lu D, Rauhauser A, Li B, Ren C, McEnery K, Zhu J, Chaki M, Vadnagara K, Elhadi S, Jetten AM, Igarashi P, Attanasio M. Loss of Glis2/NPHP7 causes kidney epithelial cell senescence and suppresses cyst growth in the Kif3a mouse model of cystic kidney disease. *Kidney international* 2016; **89**(6): 1307-23.
99. Luo F, Tao YH. Nephronophthisis: A review of genotype-phenotype correlation. *Nephrology (Carlton, Vic)* 2018; **23**(10): 904-11.
100. Luo X, Miller SD, Shea LD. Immune Tolerance for Autoimmune Disease and Cell Transplantation. *Annual Review of Biomedical Engineering* 2016; **18**(1): 181-205.
101. Luo Y, Hara T, Ishido Y, Yoshihara A, Oda K, Makino M, Ishii N, Hiroi N, Suzuki K. Rapid preparation of high-purity nuclear proteins from a small number of cultured cells for use in electrophoretic mobility shift assays. *BMC Immunol* 2014; **15**: 586-.
102. Macia MS, Halbritter J, Delous M, Bredrup C, Gutter A, Filhol E, Mellgren AEC, Leh S, Bizet A, Braun DA, Gee HY, Silbermann F, Henry C, Krug P, Bole-Feysot C, Nitschké P, Joly D, Nicoud P, Paget A, Haugland H, Brackmann D, Ahmet N, Sandford R, Cengiz N, Knappskog PM, Boman H, Linghu B, Yang F, Oakeley EJ, Saint Mézard P, Sailer AW, Johansson S, Rødahl E, Saunier S, Hildebrandt F, Benmerah A. Mutations in MAPKBP1 Cause Juvenile or Late-Onset Cilia-Independent Nephronophthisis. *American journal of human genetics* 2017; **100**(2): 323-33.
103. Mahmood T, Yang P-C. Western blot: technique, theory, and trouble shooting. *N Am J Med Sci* 2012; **4**(9): 429-34.
104. Malicki JJ, Johnson CA. The Cilium: Cellular Antenna and Central Processing Unit. *Trends in cell biology* 2017; **27**(2): 126-40.

105. Mangerich A, Burkle A. Pleiotropic cellular functions of PARP1 in longevity and aging: genome maintenance meets inflammation. *Oxidative medicine and cellular longevity* 2012; **2012**: 321653.
106. Manning CF, Bundros AM, Trimmer JS. Benefits and pitfalls of secondary antibodies: why choosing the right secondary is of primary importance. *PloS one* 2012; **7**(6): e38313.
107. Michalski A, Damoc E, Hauschild J-P, Lange O, Wieghaus A, Makarov A, Nagaraj N, Cox J, Mann M, Horning S. Mass spectrometry-based proteomics using Q Exactive, a high-performance benchtop quadrupole Orbitrap mass spectrometer. *Mol Cell Proteomics* 2011; **10**(9): M111.011015-M111.
108. Mick DU, Rodrigues RB, Leib RD, Adams CM, Chien AS, Gygi SP, Nachury MV. Proteomics of Primary Cilia by Proximity Labeling. *Developmental cell* 2015; **35**(4): 497-512.
109. Mirvis M, Stearns T, James Nelson W. Cilium structure, assembly, and disassembly regulated by the cytoskeleton. *The Biochemical journal* 2018; **475**(14): 2329-53.
110. Mitchison HM, Valente EM. Motile and non-motile cilia in human pathology: from function to phenotypes. *The Journal of Pathology* 2017; **241**(2): 294-309.
111. Mochizuki T, Wu G, Hayashi T, Xenophontos SL, Veldhuisen B, Saris JJ, Reynolds DM, Cai Y, Gabow PA, Pierides A, Kimberling WJ, Breuning MH, Deltas CC, Peters DJ, Somlo S. PKD2, a gene for polycystic kidney disease that encodes an integral membrane protein. *Science (New York, NY)* 1996; **272**(5266): 1339-42.
112. Mullis K, Faloona F, Scharf S, Saiki R, Horn G, Erlich H. Specific enzymatic amplification of DNA in vitro: the polymerase chain reaction. *Cold Spring Harbor symposia on quantitative biology* 1986; **51 Pt 1**: 263-73.
113. Nakad R, Schumacher B. DNA Damage Response and Immune Defense: Links and Mechanisms. *Frontiers in genetics* 2016; **7**: 147.
114. Nicolas E, Golemis EA, Arora S. POLD1: Central mediator of DNA replication and repair, and implication in cancer and other pathologies. *Gene* 2016; **590**(1): 128-41.
115. Omelon S, Georgiou J, Habraken W. A cautionary (spectral) tail: red-shifted fluorescence by DAPI-DAPI interactions. *Biochemical Society transactions* 2016; **44**(1): 46-9.
116. Oricchio E, Saladino C, Iacovelli S, Soddu S, Cundari E. ATM is activated by default in mitosis, localizes at centrosomes and monitors mitotic spindle integrity. *Cell cycle (Georgetown, Tex)* 2006; **5**(1): 88-92.
117. Pala R, Alomari N, Nauli SM. Primary Cilium-Dependent Signaling Mechanisms. *International journal of molecular sciences* 2017; **18**(11).
118. Pluznick JL, Caplan MJ. Chemical and Physical Sensors in the Regulation of Renal Function. *Clinical journal of the American Society of Nephrology : CJASN* 2015; **10**(9): 1626-35.
119. Poitevin Y, Pontini G, Fischer N, Kosco-Vilbois M, Elson G. Magnetic sorting of membrane associated IgG for phenotype-based selection of stable antibody producing cells. *Journal of immunological methods* 2017; **444**: 1-6.
120. Pollak MR, Quaggin SE, Hoenig MP, Dworkin LD. The glomerulus: the sphere of influence. *Clinical journal of the American Society of Nephrology : CJASN* 2014; **9**(8): 1461-9.
121. Ramachandran H, Herfurth K, Grosschedl R, Schafer T, Walz G. SUMOylation Blocks the Ubiquitin-Mediated Degradation of the Nephronophthisis Gene Product Glis2/NPHP7. *PloS one* 2015; **10**(6): e0130275.
122. Ramachandran H, Schafer T, Kim Y, Herfurth K, Hoff S, Lienkamp SS, Kramer-Zucker A, Walz G. Interaction with the Bardet-Biedl gene product TRIM32/BBS11 modifies the half-life and localization of Glis2/NPHP7. *The Journal of biological chemistry* 2014; **289**(12): 8390-401.

123. Ramachandran H, Yakulov TA, Engel C, Muller B, Walz G. The C175R mutation alters nuclear localization and transcriptional activity of the nephronophthisis NPHP7 gene product. *European journal of human genetics : EJHG* 2016; **24**(5): 774-8.
124. Ran FA, Hsu PD, Wright J, Agarwala V, Scott DA, Zhang F. Genome engineering using the CRISPR-Cas9 system. *Nature protocols* 2013; **8**(11): 2281-308.
125. Ray Chaudhuri A, Nussenzweig A. The multifaceted roles of PARP1 in DNA repair and chromatin remodelling. *Nature Reviews Molecular Cell Biology* 2017; **18**: 610.
126. Reiter JF, Leroux MR. Genes and molecular pathways underpinning ciliopathies. *Nature Reviews Molecular Cell Biology* 2017; **18**: 533.
127. Robbins DJ, Fei DL, Riobo NA. The Hedgehog signal transduction network. *Science signaling* 2012; **5**(246): re6.
128. Robertson GL, Norgaard JP. Renal regulation of urine volume: potential implications for nocturia. *BJU international* 2002; **90 Suppl 3**: 7-10.
129. Rohatgi R, Milenkovic L, Scott MP. Patched1 regulates hedgehog signaling at the primary cilium. *Science (New York, NY)* 2007; **317**(5836): 372-6.
130. Sanchez I, Dynlacht BD. Cilium assembly and disassembly. *Nature cell biology* 2016; **18**(7): 711-7.
131. Slaats GG, Braun F, Hoehne M, Frech LE, Blomberg L, Benzing T, Schermer B, Rinschen MM, Kurschat CE. Urine-derived cells: a promising diagnostic tool in Fabry disease patients. *Scientific reports* 2018; **8**(1): 11042.
132. Slaats GG, Giles RH. Are renal ciliopathies (replication) stressed out? *Trends in cell biology* 2015; **25**(6): 317-9.
133. Slaats GG, Saldivar JC, Bacal J, Zeman MK, Kile AC, Hynes AM, Srivastava S, Nazmutdinova J, den Ouden K, Zagers MS, Foletto V, Verhaar MC, Miles C, Sayer JA, Cimprich KA, Giles RH. DNA replication stress underlies renal phenotypes in CEP290-associated Joubert syndrome. *The Journal of clinical investigation* 2015; **125**(9): 3657-66.
134. Srivastava S, Molinari E, Raman S, Sayer JA. Many Genes—One Disease? Genetics of Nephronophthisis (NPHP) and NPHP-Associated Disorders. *Frontiers in Pediatrics* 2018; **5**(287).
135. Starczewska E, Beyaert M, Michaux L, Vekemans M-C, Saussoy P, Bol V, Arana Echarri A, Smal C, Van Den Neste E, Bontemps F. Targeting DNA repair with aphidicolin sensitizes primary chronic lymphocytic leukemia cells to purine analogs. *Oncotarget* 2016; **7**(25): 38367-79.
136. Steinberg TH. Protein gel staining methods: an introduction and overview. *Methods in enzymology* 2009; **463**: 541-63.
137. Stokman M, Lilien M, Knoers N. Nephronophthisis. In: Adam MP, Ardinger HH, Pagon RA, et al., eds. GeneReviews(®). Seattle (WA): University of Washington, Seattle Copyright © 1993-2020, University of Washington, Seattle. GeneReviews is a registered trademark of the University of Washington, Seattle. All rights reserved.; 1993.
138. Terpe K. Overview of bacterial expression systems for heterologous protein production: from molecular and biochemical fundamentals to commercial systems. *Applied Microbiology and Biotechnology* 2006; **72**(2): 211.
139. Tomomori-Sato C, Sato S, Conaway RC, Conaway JW. Immunoaffinity purification of protein complexes from Mammalian cells. *Methods Mol Biol* 2013; **977**: 273-87.
140. Trolle T, McMurtrey CP, Sidney J, Bardet W, Osborn SC, Kaever T, Sette A, Hildebrand WH, Nielsen M, Peters B. The Length Distribution of Class I-Restricted T Cell Epitopes Is Determined by Both Peptide Supply and MHC Allele-Specific Binding Preference. *J Immunol* 2016; **196**(4): 1480-7.

141. Tsvetkov L, Xu X, Li J, Stern DF. Polo-like kinase 1 and Chk2 interact and co-localize to centrosomes and the midbody. *The Journal of biological chemistry* 2003; **278**(10): 8468-75.
142. Tukachinsky H, Lopez LV, Salic A. A mechanism for vertebrate Hedgehog signaling: recruitment to cilia and dissociation of SuFu-Gli protein complexes. *The Journal of cell biology* 2010; **191**(2): 415-28.
143. Tyanova S, Temu T, Sinitcyn P, Carlson A, Hein MY, Geiger T, Mann M, Cox J. The Perseus computational platform for comprehensive analysis of (prote)omics data. *Nature methods* 2016; **13**(9): 731-40.
144. Valdes-Sanchez L, De la Cerda B, Diaz-Corrales FJ, Massalini S, Chakarova CF, Wright AF, Bhattacharya SS. ATR localizes to the photoreceptor connecting cilium and deficiency leads to severe photoreceptor degeneration in mice. *Human molecular genetics* 2013; **22**(8): 1507-15.
145. Vasanth S, ZeRuth G, Kang HS, Jetten AM. Identification of nuclear localization, DNA binding, and transactivating mechanisms of Kruppel-like zinc finger protein Gli-similar 2 (Glis2). *The Journal of biological chemistry* 2011; **286**(6): 4749-59.
146. Walz G. Role of primary cilia in non-dividing and post-mitotic cells. *Cell and tissue research* 2017; **369**(1): 11-25.
147. Ward CJ, Yuan D, Masyuk TV, Wang X, Punyashthiti R, Whelan S, Bacallao R, Torra R, LaRusso NF, Torres VE, Harris PC. Cellular and subcellular localization of the ARPKD protein; fibrocystin is expressed on primary cilia. *Human molecular genetics* 2003; **12**(20): 2703-10.
148. Willey CJ, Blais JD, Hall AK, Krasa HB, Makin AJ, Czerwiec FS. Prevalence of autosomal dominant polycystic kidney disease in the European Union. *Nephrology, dialysis, transplantation : official publication of the European Dialysis and Transplant Association - European Renal Association* 2017; **32**(8): 1356-63.
149. Yu FX, Guan KL. The Hippo pathway: regulators and regulations. *Genes & development* 2013; **27**(4): 355-71.
150. Zannini L, Delia D, Buscemi G. CHK2 kinase in the DNA damage response and beyond. *Journal of molecular cell biology* 2014; **6**(6): 442-57.
151. Zhang F, Jetten AM. Genomic structure of the gene encoding the human GLI-related, Kruppel-like zinc finger protein GLIS2. *Gene* 2001; **280**(1-2): 49-57.
152. Zhang F, Nakanishi G, Kurebayashi S, Yoshino K, Perantoni A, Kim YS, Jetten AM. Characterization of Glis2, a novel gene encoding a Gli-related, Kruppel-like transcription factor with transactivation and repressor functions. Roles in kidney development and neurogenesis. *The Journal of biological chemistry* 2002; **277**(12): 10139-49.
153. Zhang S, Hemmerich P, Grosse F. Centrosomal localization of DNA damage checkpoint proteins. *Journal of cellular biochemistry* 2007; **101**(2): 451-65.
154. Zhao X, Li G, Liang S. Several affinity tags commonly used in chromatographic purification. *Journal of analytical methods in chemistry* 2013; **2013**: 581093.

7. Supplements

7.1. Figures

7.2. Tables

7.3. GO-term enrichment analysis (biological processes)

Name	**Score**
actin filament bundle assembly	0,858251
regulation of protein secretion	0,859478
inhibition of adenylate cyclase activity by G-protein signaling pathway	0,853565
cellular response to glucagon stimulus	0,827096
negative regulation of adenylate cyclase activity	0,820424
negative regulation of cyclase activity	0,820424
negative regulation of lyase activity	0,820424
positive regulation of actin filament bundle assembly	0,820133
positive regulation of stress fiber assembly	0,820133
regulation of actin filament bundle assembly	0,820133
regulation of stress fiber assembly	0,820133
regulation of adenylate cyclase activity	0,810306
regulation of cyclase activity	0,810306
regulation of lyase activity	0,810306

actin polymerization or depolymerization	0,802404
regulation of cAMP biosynthetic process	0,790687
regulation of cyclic nucleotide biosynthetic process	0,790687
regulation of nucleotide biosynthetic process	0,790687
cAMP-mediated signaling	0,799651
G-protein signaling, coupled to cAMP nucleotide second messenger	0,799651
positive regulation of neuron projection development	0,78631
lymphocyte costimulation	0,777003
T cell costimulation	0,777003
positive regulation of stress-activated protein kinase signaling cascade	0,797795
ruffle organization	0,795764
renal system process	0,776037

7.4. Overlap of the GLIS2 interactome with published ciliary proteomes

Protein name	Kohli et al.	Mick et al.
MAP4	+	+
CDC42	+	+
CALR	+	+
CTNNA1	+	+
CTTN	+	+
ACTN1	+	+
ACTN4	+	+
TJP2	+	+
PDIA6	+	+
EZR	+	+
EIF4B	+	+
VCP	+	+
RAC1	+	+
RHOA	+	+
MACF1	+	+
SEPT2	+	+
SEPT7	+	+
SEPT11	+	+
MARCKS	+	
DYNNLL2	+	
YES1	+	
HSP90B1	+	
CORO1C	+	
CANX	+	
RAI14	+	
PACSIN2	+	
CTNNB1	+	
CTNND1	+	
LSR	+	
SNAP23	+	
TJP1	+	
P4HB	+	
PDIA3	+	
PDIA4	+	
CXADR	+	
GANAB	+	

PRKCSH	+	
DLG1	+	
PPP1R12A	+	
SCRIB	+	
AKAP12	+	
RAP1A	+	
PLEKHA7	+	
BASP1	+	
FLNA	+	
PRDX2	+	
SLC1A5	+	
PPP1CA	+	
NCKAP1	+	
GNB1	+	
RRAS2	+	
RHOC	+	
DSC2	+	
CLTC	+	
TOAK1	+	
ARF6	+	
SAMHD1	+	
EEF1D	+	
TPM4	+	
SPECC1	+	
FARP1	+	
RAB1B		+
COPG1		+
PPP2R1A		+
ADD3		+
UBAP2L		+
KHSRP		+
AIMP2		+
POLD1		+
PDCD6IP		+
GOT2		+

SQSTM1	+	
ALDOA	+	
PAICS	+	
MYCBP2		+
CORO1B		+
ANAX6		+
CAPZB		+
DSG2		+
UBA1		+
TARS		+
EPB41L3		+
RRM1		+
IMPDH2		+
ATP6V1A		+
PTGES3		+
TPM3		+
NME1		+
STIP1		+
PRNP		+
LDHB		+
GPI		+
GDI2		+
MYO1C		+
GPC1		+

PPA1		+
GNAS		+
TPO1		+
PPP1CC		+
AP2A1		+
EIF3A		+
HSPA4		+
ACYL		+
CHORDC1		+
ST13		+
PSMC3		+
MSN		+
GSN		+